THE EFFECTS OF POLYMER/SURFACTANT ADDITIVES ON THE FLOW AND HEAT TRANSFER AROUND A CIRCULAR CYLINDER IN PERIODIC VORTEX SHEDDING

by

Çağlar Şahin

B.S., Mechanical Engineering, Istanbul Technical University, 2014

Submitted to the Institute for Graduate Studies in
Science and Engineering in partial fulfillment of
the requirements for the degree of
Master of Science

Graduate Program in Mechanical Engineering
Boğaziçi University

2018

ACKNOWLEDGEMENTS

First of all, I would like to sincerely thank my thesis supervisor Prof. Kunt Atalık for his support, guidance and expertise throughout my thesis study.

I would like to thank each of my friends with whom I had a good time through my graduate study.

Lastly, I am grateful to my parents for their endless support and love.

This thesis has been supported by Boğaziçi University Research Fund with grant number 11821.

ABSTRACT

THE EFFECTS OF POLYMER/SURFACTANT ADDITIVES ON THE FLOW AND HEAT TRANSFER AROUND A CIRCULAR CYLINDER IN PERIODIC VORTEX SHEDDING

This study focuses on the flow and heat transfer properties of dilute polymer/surfactant solutions using Newtonian, and inelastic/elastic non-Newtonian constitutive models. The results are discussed in terms of drag and lift coefficients, vortex shedding frequency, vortex formation length, separation angle, the critical Reynolds number for the onset of vortex shedding, local and average Nusselt numbers. Drag reduction is observed for shear thinning fluids; moreover, the vortex shedding frequency increases, and the vortex formation length decreases under shear thinning. Fluid elasticity leads to an increase in the drag coefficient and vortex formation length, and a decrease in the vortex shedding frequency and separation angle. The onset of vortex shedding is earlier under shear thinning whereas it is delayed under shear thickening. It is also observed that weakly elastic effects have almost no impact on the onset of periodic vortex shedding. Blockage effect causes to increase time-averaged drag coefficient and Strouhal number and it delays the onset of laminar vortex shedding for Newtonian and shear thickening fluids. For non-isothermal flow condition, heat transfer enhancement is observed under inelastic shear thinning effects through an increase of the local and average Nusselt numbers, however purely viscoelastic effects lead to a decrease in the rate of convective heat transfer for the studied range of parameters. Temperature gradients decrease in the wake region under elasticity whereas shear thinning leads to an increase in the gradients and to the formation of elongated and clustered isotherms.

ÖZET

POLİMER/YÜZEY AKTİF MADDE KATKISININ PERİYODİK GİRDAP KOPMASINDA DAİRESEL SİLİNDİR ETRAFI AKIŞA VE ISI TRANSFERİNE ETKİLERİ

Bu çalışma Newtonyen ve Newtonyen olmayan inelastik/elastik bünye modelleriyle, seyreltik polimer/yüzey aktif madde katkılı çözeltilerin akış ve ısı transferi özelliklerinin incelenmesini hedeflemektedir. Sonuçlar kaldırma ve sürükleme katsayıları, girdap kopma frekansı, girdap oluşum uzaklığı, ayrılma açısı, girdap kopmasının başladığı kritik Reynolds sayısı, yerel ve ortalama Nusselt sayısı gibi parametreleri cinsinden incelenmiştir. Kayma incelmesi gösteren akışkanın sürükleme katsayısında azalma gözlemlenirken, girdap kopma frekansında artış ve girdap oluşum uzaklığında azalma görülmektedir. Elastik etkiler sürükleme katsayısında ve girdap kopma frekansında artışa, girdap kopma frekansı ve ayrılma açısında ise azalmaya yol açmaktadır. Girdap kopma başlangıcı kayma incelmesi altında daha erken, kayma kalınlaşması altında ise daha geç gözlemlenmektedir ve düşük elastik etkilerin girdap kopmasının başlangıcına etki etmediği görülmüştür. Duvar etkisinin ise zaman ortalaması alınmış sürükleme katsayısına ve Strouhal sayısına arttırıcı etkisi vardır. Girdap kopma hareketi duvar etkisiyle Newtonyen ve kayma kalınlaşması gösteren akışkanlar için daha yüksek Reynolds sayılarında gözlemlenirken, kayma incelmesi gösteren akışkanlarında daha düşük Reynolds sayılarında gözlemlenmektedir. Eşısıl olmayan akış koşullarında, lokal ve ortalama Nusselt sayıları dikkate alındığında, taşınımla ısı geçişi arttırımında kayma incelmesinin önemli rol oynadığı, öte yandan elastik etkilerin taşınımla ısı geçişi hızını azalttığı gözlemlenmiştir. Elastik davranışın artışı eş sıcaklık yapılarında küçülmeye sebep olmuş, artan kayma incelmesi ise geniş ve kümelenmiş eş sıcaklık eğrilerinin oluşmasına katkıda bulunmuştur.

TABLE OF CONTENTS

LIST OF FIGURES

LIST OF TABLES

LIST OF SYMBOLS

B	Blockage ratio
c_p	Specific heat capacity
C_D	Drag coefficient
C_L	Lift coefficient
D	Diameter of the cylinder
De	Deborah number
$\overline{\overline{D}}$	Rate of deformation tensor
K	Degrees Kelvin
L	Extensibility parameter
L_f	Vortex formation length
m	Consistency factor
Nu	Local Nusselt number
$\overline{Nu}$	Average Nusselt number
n	Power-law index
p	Pressure
Pr	Prandtl number
Re	Reynolds number
St	Strouhal number
t	Time
T	Temperature
$\overline{\overline{T}}$	Stress tensor
$\overline{\overline{T_1}}$	Viscoelastic component of the stress tensor
$\overline{\overline{T_2}}$	Purely viscous component of the stress tensor
u	Longitudinal velocity fluctuations
U	Local mean velocity
U_∞	Freestream velocity
v	lateral velocity fluctuations
$\boldsymbol{V}$	Velocity

Wi	Weissenberg number
α	Mobility factor
β	Viscosity ratio
$\dot{\gamma}$	Shear rate
η	Dynamic viscosity
θ_s	Separation angle
μ	Micro
ρ	Density

LIST OF ACRONYMS/ABBREVIATIONS

2D	Two Dimensional
3D	Three Dimensional
CFD	Computational fluid dynamics
CMC	Carboxymethyl cellulose
CTAB	Cetyltrimethyl ammonium bromide
LDV	Laser Doppler velocimetry
PEO	Polyethylene oxide
PIV	Particle image velocimetry
pH	Potential of hydrogen
ppm	Parts per million
rms	Root mean square
wppm	Weight parts per million

1. INTRODUCTION

Friction factor and drag coefficient are known to be reduced under polymer/surfactant addition in turbulent flow regime for internal and external flows which have many applications such as oil pipeline systems, heat exchangers, oil well fracturing operations, hydrotransport processes and biomedical flows [1].

Since 1940's, adding a small amount of additive such as polymer or surfactant has been used for reduction in friction in turbulent pipe flow which is classified as drag reduction; moreover, adding small amount (100 ppm) of long-chain polymer molecules could reduce turbulent skin friction drag by 80% [2]. After that, polymer additives were used commercially for the first time in Trans Alaska crude oil pipeline systems in order to increase the flow rate and obtain efficient operation in 1979 [3]. Furthermore, Gadd studied relation between vortex street formation of immersed body and polymer addition [4]. Generally, drag reduction increases with increasing polymer concentration, polymer molecular weight, Reynolds number and flow rate; however, some parameters such as channel size, geometry, pH, temperature, surface roughness, concentration influence the performance of drag.

In 1980, Fabula *et al.* [5] from the United States Navy took out a patent of torpedo drag reduction employing polymer ejection. Ambient water (seawater) is ingested and mixed with the concentrated polymer, then produced seawater-polymer solution is ejected from the nose of torpedo backwardly in contact with the surface of the torpedo. Almost 37% drag reduction was achieved with 1.8 gal/sec ejection flow rate and 0.2% polymer concentration.

Unlike additive techniques for drag reduction, non-additive techniques on geometry such as riblets, dimples, oscillating walls and micro-bubbles and provide a fair amount of drag reduction in certain applications. Riblets are protrusions, which resembles to shark fin, with different shapes like V-shaped and U- shaped. Turbulent intensity of flow might be reduced up to 6-10% which is much lower than additive

techniques using riblets; however, the mechanisms underlying the drag reduction of riblets are still unclear. Discrete indentations onto the surface to reduce turbulent skin-friction up to 20% are called dimples which are commonly used in golf balls. Generation of spanwise or streamwise oscillation with walls also promotes turbulent drag reduction up to 40% . Spanwise vorticities assist to decrease of drag force by means of reduction in near-wall velocity gradient. Similarly, microbubbles with diameter around $10\mu m$ produced by electrolysis or different ways are effective for drag reduction. Despite being environmental friendly, these non-additive techniques are less used because of their implementation costs and relatively low achievable drag reduction [1].

The presence of polymer/surfactant additives in the base fluid (water) causes to a different rheological behavior compared to pure water such as decreasing viscosity with increasing shear rate, and viscoelasticity. Therefore, Newtonian constitutive model is generally not applicable for these solutions.

1.1. Rheology

In 1920, the term "rheology" which means the theory of deformation and flow of matter was officially invented by Markus Reiner and Eugene Bingham. The concept of rheology comprises the rigid solid (The Euclidean solid) to ideal inviscid fluid (Pascalian fluid) which are ideally identified terms [6].

Newtonian fluids have a constant viscosity under changing shear rate at constant temperature and pressure whereas the fluids which have non-linear shear stress curve with changing shear rate are called non-Newtonian fluids. Water, alcohol and air are examples of Newtonian fluids, also polymer solutions, biological and drilling fluids are typical examples for non-Newtonian fluids. Purely viscous or inelastic, time-dependent and viscoelastic fluids can be subcategorized classes of non-Newtonian fluids [6].

Purely viscous or inelastic fluids can be described as shear-thinning or pseudoplastic if the viscosity decreases with increasing rate of shear, on the contrary fluids have the viscosity that increases with increasing rate of shear are named as shear-thickening

(dilatant) fluids. Most of the non-Newtonian fluids show shear-thinning behavior in real life. In literature, presented several models, which are varied from each other with required number and type of parameters, for Generalized Newtonian fluids (inelastic fluids) have been used to obtain analytical solutions. These models are produced from experimental data and theoretical basis. Power- law, Bird-Carreau, Cross Law and Carreau-Yasuda Law are some examples of the constitutive models for non-Newtonian inelastic fluids [6].

Time dependent fluids are more complex and difficult to model. Their viscosity either decreases or increases monotonically depending on duration of shearing and their kinematic history. The conventional shear stress-shear rate curves have restricted capabilities unless kinematic history of samples are known [7].

On the other hand, both elastic solids and ideal fluids behavior are the feature of viscoelastic fluids. Because of the complexity of viscoelastic fluid which has blend of fluid-like and solid-like responses under suitable conditions, it is quite difficult to solve mathematical equations according to the behavior of the real fluid. Three important models, Maxwell, Kelvin-Voigt and Burger, related to usage of springs and dashpots were applied to observe viscous and elastic effects [8]. Memory effect is the distinctive property of viscoelastic fluids, and relaxation time (λ) is a significant parameter which address to time required for viscoelastic substance to relax from a stressed state to its initial state. Relaxation time is limited between zero and infinity in order to correspond viscous to elastic response. Whereas low relaxation time implies memory loss, high relaxation time corresponds high memory retention of the flow [9].

1.2. Literature Review

Flow around a circular cylinder has been a crucial problem in fluid mechanics for both experimental and numerical studies from last decades. Many practical applications have been carried out related to this topic in automotive, aircraft and construction industries. Simplification of a geometry as a cylinder is quite common for investigating bluff body aerodynamics and internal/external flow properties, also investigating of

simplified geometry is more applicable and accurate than complicated real geometry.

1.2.1. Isothermal Studies for Flow Around Cylinder with Polymer/ Surfactant Additives

1.2.1.1. Experimental Studies. In the literature, there are quite restricted studies about polymer/surfactant added fluid flow over a circular cylinder in the laminar and transition regime.

Gadd [4] claimed the reduction of Strouhal Number by increasing concentration of polyethylene oxide (PEO) - water solution 10 to 40 wppm at Reynolds number $Re = 240$. It was also stated that 10 wppm, below which no any change of the vortex frequency occurs, is determined as threshold concentration for polyethylene oxide (PEO).

Kalashnikov and Kudin [10] experimentally investigated amplitude and oscillations of water, PEO and Guar gum solutions for Reynolds number $Re < 400$ and up to 100 wppm. PEO solution was passed through the centrifugal pump so as to obtain inelastic associate-containing solution. It is concluded that the frequency of the Karman vortex and the intensity of inertial vortices increases in inelastic solutions, whereas it decreases in elastic ones compared with the Newtonian case.

Usui *et al.* [11] found out that not only increasing polymer addition but also decrease of cylinder diameter suppress the Karman vortex formation. In addition, they found an empirical correlation between Strouhal (St) and Weissenberg number (Wi). An alternative parameter was also discussed, $D/\sqrt{\lambda v}$, instead of Weissenberg number to explain effect of polymer additive on the vortex formation. It was deduced that $D/\sqrt{\lambda v}$ term might be more feasible than Wi in case of high Reynolds numbers.

Effects of dilute cationic surfactant solutions (1000 ppm) on the flow around a circular cylinder were studied by Bergins *et al.* [12] for Reynolds number 110 to 2000. They used both LDV and Schlieren optics for monitoring flow structure, and they

found out that exceeding a critical Reynolds number which depends on the age of the solution reduces the vortex shedding frequency. In addition, the wake structure and vortex shedding frequency do not considerably change for the Reynolds number below 200 in comparison with water.

Experimental work of Ozgoren [13] in 2005 investigated that the flow (Newtonian) around a circular and square cylinder with two different positions (sharped-edge square and 45 degree orientated square). It has been found that values of Strouhal number, as well as wake patterns, are functions of the cross-section of the cylinder and Reynolds numbers, also this study has supported the previous works.

Rehimi *et al.* [14] experimentally investigated wall confinement effect on the wake formation behind a circular cylinder for $B = 1/3$ by using 2D PIV measurements. They found that the von Karman instability is delayed to Reynolds number $Re = 108$ from $Re = 47$ which is the condition of unconfined cylinder case. Although wavelength of the von Karman vortices is about $5D$ to $6D$ for the unconfined cylinder case, they obtained $3D$ for $1/3$ blockage case. They also investigated stabilizing impacts of walls on mean recirculation region and rms velocities. In addition, same as Williamson's study [15], Mode A and Mode B 3D instabilities are observed at Reynolds number $Re = 159$ and $Re = 230 - 260$ respectively.

He, Li and Wang [16] presented an experimental study of flow around square cylinders with cut-corners at the front edges by using PIV. They stated that drag reduction can be achieved for the cut-corner dimensions at Reynolds number of 1035 for Newtonian fluid. While direct proportionality between drag coefficient and the minimum wake width is observed, it is seen that the vortex shedding frequency is inversely proportional to the minimum wake width. It is also revealed that cut-corners at the front edges can reduce both the size and strength of wake vortex leading to suppression of separation over the surface.

In recent experimental observations on flow past a cylinder by Coelho and Pinho [17] 0.2, 0.3, 0.4 and 0.6 wt. % concentration of tylose-water solutions were used as weakly elastic fluids, and 0.1, 0.2,0.3 and 0.4 wt. % concentration of cellulose sodium salt (CMC) solutions were used as more elastic fluid over the range $50 < Re < 9000$, based on a length scale twice the diameter of the cylinder. Elastic and shear thinning characteristics of solutions increase with increasing additive concentration; furthermore, shear thinning behavior was seen all the solutions by fitting to the Carreau-Yasuda and power-law viscosity models. The laminar vortex shedding was investigated only for 0.3 and 0.4 % concentrated solutions, and several Reynolds number definitions had been suggested to mark the onset and end of the diverse flow regimes. The characteristic shear rate, $U_\infty/2D$, was used for the viscosity and Reynolds number calculations. As a result, they found out that aspect ratio and fluid elasticity give rise to reduction of several critical Reynolds numbers which individually indicate end of the transition regime, sudden drop in vortex formation and the base of the peak frequency in the power spectra becomes narrower by degree. The transition regime is encountered earlier and even suppressed for the 0.6 % tylose solution by fluid elasticity. Furthermore, fluid elasticity can be better examined with elasticity number which is Re/Wi than Weissenberg number. In elasticity number, viscosity is calculated by using a high characteristic shear rate rather than the average value which is $U_\infty/2D$.

Coelho and Pinho [18] deduced that shear-thinning brings about the reduction of the diffusion length and the boundary layer thickness, to a raise in the vortex shedding frequency, i.e. the Strouhal number. However, fluid elasticity is responsible for an enhancement in the formation length, which in turn leads to a decrease in the shedding frequency. Experimental results for the tested solutions show an increase in Strouhal number with increasing polymer concentration. Furthermore, the critical formation length which implies the value of formation length just prior to its sudden drop increases with increasing Weissenberg number as elasticity decreases the entrainment of fluid by the shear layers from the formation region.

The pressure (form) drag reduction was observed with increasing polymer concentration for Reynolds number below $Re = 800$ and this behavior attributed to fluid

elasticity on the shear layers by Coelho and Pinho [19]. Pressure rise coefficient which is difference between the base and minimum pressure coefficients has no notable influence on the critical Reynolds numbers and formation length. Straight correlation was found between the elasticity number and the mean pressure rise coefficient.

The effect of viscoelastic Ethoquad O/12 (oleyl- bihydroxyethyl- methyl- ammonium -chloride) surfactant solutions on the flow past a circular cylinder was experimentally and numerically investigated for the Reynolds number ranging from $Re = 10$ to $Re = 10^5$ by Ogata *et al.* [20]. They observed that the drag coefficient increases compared to that of tap water for $10 < Re < 3000$; however, drag is reduced for $3000 < Re < 30000$, and the maximum drag reduction occurs at $Re = 7000$ up to %55 for 200 ppm surfactant solution. Existence of wide stagnation zone around the cylinder and increase of cylinder's diameter are other presented reasons of drag. Drag reduction is also associated with narrowing wake at the rear of the cylinder at higher Reynolds numbers.

Effects of small amount of elasticity on 2D laminar vortex shedding instability, the fluctuating and time-averaged velocity fields were investigated experimentally in the Reynolds number range $50 < Re < 150$ and Weissenberg number range $0.3 < Wi < 0.8$ by Pipe and Monkewtiz [21]. They observed a decrease in the Karman vortex shedding frequency for the low concentration aqueous solutions of polyethylene oxide (PEO) due to elasticity. However, at higher concentrations, they observed an increase in the shedding frequency due to increasing shear thinning effects. Their laser doppler anemometry (LDA) measurements showed that the transverse velocity fluctuations on the wake centerline were similar to the Newtonian case at low concentrations although a reduction in strength is noted at their highest concentrations. They argued that the normal stress differences and the elongational viscosity contribute to the development of flow instability.

A mixture of polymer and surfactant is also known as a good drag reducer. From the work done by Kim *et al.* [22], it can be deduced that adding surfactant to polymeric solution increases drag reduction efficacy, and polymer concentration plays an

important role in drag reduction for polymer/surfactant solutions. The maximum drag reduction is provided with the critical polymer concentration, however the drag reduction efficacy decreases faster than that of pure polymeric solution when the critical concentration exceeded. In addition, Matras *et al.* [23] stated that poly-ethylene oxide (PEO) and cetyltrimethyl ammonium bromide (CTAB) solution reduces drag much more than solutions with these substances alone in a pipe flow for laminar to turbulent regime of surfactant solution with salt and for turbulent flow regime of polymer solution. They also emphasize that polymer-surfactant solution is able to show strong drag reduction even after degradation.

1.2.1.2. Numerical Studies. It is well known that solutions with polymer/surfactant additives exhibit more complex rheological behavior than Newtonian fluids, due to non-Newtonian effects such as shear thinning, anisotropy and viscoelasticity. In spite of their wide occurrence, only few numerical studies have been reported on the flow of non-Newtonian fluids past bluff bodies.

Patnana *et al.* [24] numerically investigated the unsteady flow of incompressible power-law fluids over an unconfined circular cylinder between the Reynolds number 40 and 140. They presented detailed kinematics of the flow and macroscopic parameters (the drag and lift coefficients, Strouhal number). It was concluded that the flow transits from steady to unsteady behavior at a critical value of Reynolds number $Re \sim 40 - 50$ depending upon the value of the power-law index. Both the lift coefficient and Strouhal number were zero for the steady flow regime, however; in the unsteady regime, they rose with the increasing Reynolds number. Unsteadiness in the flow was determined at $Re = 50$ for all values of power-law index (n). Kinematics of the flow and periodic vortex shedding status demonstrate complex regime after critical Reynolds number, and for a fixed Reynolds number, the drag coefficient values rise with the increasing power law index (n). Moreover, for a constant power-law index (n), the drag coefficient steadily declines with Reynolds number. Increasing value of power-law index also reduces the lift coefficient values. Strouhal number decreases with rising value of power-law index at any constant Reynolds number between $Re = 40$ and $Re = 140$. Soares

et al. [25] also investigated the non-Newtonian flow across a heated circular cylinder numerically that the frictional drag component increased with the flow-behavior index n and the dependence of this component on n increased with Reynolds number.

Sivakumar *et al.* [26] conducted transient numerical investigation about effect of power-law index on the critical Reynolds number for 2D steady to unsteady flow around an unconfined circular cylinder over a range of power-law index ($0.3 \leq n \leq 0.8$). Stabilizing influence on the flow is observed in shear thinning fluids, and increasing shear thickening behavior is prone to induce asymmetry. Critical time-averaged mean drag coefficient, Strouhal and Reynolds numbers are expressed by numerical expressions in terms of power-law index.

The steady and incompressible flow of power-law fluids past a circular cylinder is investigated numerically for power law index $0.2 \leq n \leq 1.2$, for blockage ratios $B = 0.037, 0.082, 0.164$, for Reynolds numbers $Re = 1, 20, 40$ with a stream function/vorticity formulation by Chhabra *et al.* [27]. They found a critical power law index, reducing with Reynolds number (inversely proportional), which makes the drag coefficient independent of blockage ratio. A high blockage ratio brings about an increase in drag alongside a decrease in separation angle for $n > 0.9$. Furthermore, Rao *et al.* [28] worked on numerical simulations of the 2D laminar flow of power-law fluids over elliptical cylinders with different aspect ratios, and they demonstrated that the power-law index is increased from 0.3 to 1.8; the drag coefficient raises continuously with Reynolds number between 30 and 200. The two-dimensional and unsteady free stream flow of power law fluids past a square cylinder investigated numerically by Sahu *et al.* [29] in the range of $60 \leq Re \leq 160$ and $0.5 \leq n \leq 2.0$. They obtained that no leading edge separation is seen to occur in shear-thickening fluids, at least in the observed range of Reynolds number and power law index. While the drag coefficient decreases with the increasing Reynolds number in shear-thickening fluids, because of the occurring recirculation on the surface of the cylinder in shear-thinning fluids, the drag coefficient goes up with the increasing Reynolds number.

The effects on the fluid tunnels by confining walls has been termed as blockage, and the blockage ratio is defined as $B = D/H$, where D is the cylinder diameter and H is the height between lateral walls. There are quite few experimental studies about wall effects on drag reduction and wake formation, also relatively more numerical studies in literature.

Anagnostopoulos and Iliadis [30] studied blockage effects on the viscous flow past a circular cylinder numerically at Reynolds number $Re = 106$ for blockage ratios of 0.05, 0.15, 0.25. As the blockage ratio increases,the Strouhal number, the separation angle and drag force increase considerably. Nevertheless, 90% increase of the fluctuating lift force is observed by increasing blockage 0.05 to 0.25. Similarly, steady-state numerical computations was carried out by Chakraborty *et al.* [27] with blockage ratio range $0.05 \leq B \leq 0.65$ and Reynolds number range $0.1 \leq Re \leq 200$. They showed that both separation angle and length of the recirculation region decreases with increasing blockage ratio, and total drag coefficient increases with increasing wall confinement because of a significant increase in pressure drag.

Sahin and Owens [31] studied wall proximity effect on flow past a circular cylinder in Reynolds number $0 < Re \leq 280$ and in blockage ratio $0.1 < B \leq 0.9$, and they found out at least three different neutral stability curves for $B \leq 0.9$. Alongside the neutral stability curves, they presented increasing drag coefficient and the critical Reynolds number for the primary instability as blockage ratio increases. Kumar and Mittal [32] also showed increasing both the critical Reynolds number for the onset of laminar vortex shedding and the vortex shedding frequency with increasing blockage ratio by using linear stability analysis.

A Floquet stability analysis and empirical formulation were used to investigate the dynamics of the periodic 2D flow past a circular cylinder confined in a channel by Griffith *et al.* [33] They studied in Reynolds number $0 < Re \leq 200$ and in blockage ratio $0.1 \leq B \leq 0.9$, and emphasized that 2D beating phenomenon is observed for the blockage ratio 0.5 at a Reynolds number lower than any Reynolds number where mode-B type instability is seen. It was also found that the vortex shedding frequency

is increased with increasing blockage ratio.

Huang and Feng [34] also studied 2D steady flows of a viscoelastic fluid past a circular cylinder numerically for the Reynolds number between 0.1 and 10, and their results indicated that the wall effect shortens the wake and increases the drag; however, this effect was reduced by fluid elasticity. For small blockage ratios, elasticity increases the drag and lengthens the wake for all Reynolds number that was tested. Shear-thinning decreases the drag and shortens the wake for all Weissenberg Numbers, blockage ratios and Reynolds Number they tested.

A fairly detailed investigation with finite-volume method for the simulation of time-dependent viscoelastic flows over a circular cylinder was carried out by Oliveira [35] within the Reynolds number range of $50 < Re < 120$ and the Deborah number range of $0 < De < 80$, using constant viscosity FENE-CR model. He claimed both the vortex formation length and the shedding period are increased with fluid elasticity, and the vortex formation length can be extended more by increasing extensibility parameter (L^2 was investigated from 100 to 1200) of the constitutive model. Polymer addition to a Newtonian solvent also leads to reduction in root mean square (rms) of lateral velocities, and this may be cause to drag reduction.

Drag enhancement and drag reduction regimes are discussed numerically by Xiong *et al.* [36], detail along with their flow properties such as the pattern of vortex-shedding, the variation of lift as well as changes in pressure, elongational rates, and polymer stress profiles at a blockage $B = 0.1$, using the Oldroyd-B constitutive model. When the Reynolds number is smaller than the transitional Reynolds number ($Re = 40$), the drag increases as the Weissenberg number (Wi) increases in this case. In addition, they observed three different regimes which are drag reduction, drag enhancement and Newtonian drag for Reynolds number higher than 40. As the relaxation time of fluid increases, numerical simulations and soap film experiments show that the fluid elasticity may lead to flow instabilities. They drew the drag map of the cylinder in an adequate Reynolds- Weissenberg parameter space. Two threshold Weissenberg numbers as a function of Reynolds number used to identify behavior of the drag. Drag behaves

likewise Newtonian drag up to first threshold Weissenberg number, and drag reduction is observed between first and second thresholds. Above second threshold Wi, drag enhancement of the cylinder increases as the Weissenberg number increases and can be reached 250% . Xiong *et al.* also concluded that the drag reduces with increasing Weissenberg number for high Reynolds number polymer solutions till drag reduction reaches its maximum point, which is around %50 drag reduction; and after that point, increasing Weissenberg number has an adverse effect that gives rise to an increase in the drag coefficient.

The numerical simulation of the transient two-dimensional inertial viscoelastic flow around a circular cylinder was investigated at Reynolds number $Re = 100$ and Weissenberg number $Wi = 80$ by Norouzi *et al.* [37]. Giesekus constitutive model was used to compare the results of FENE-CR and Newtonian fluid models. The results reveal that fluid elasticity induces an increase in the size of recirculation region and a decrease in the amplitude and vortex shedding frequency. They also investigated the impact of mobility factor on the flow stability, and it was concluded that increasing the mobility factor results in a significant increase in the vortex shedding frequency and flow instability.

In addition, Rao *et al.* [38] studied the role of wall confinement on the flow of power-law fluids past a circular cylinder numerically for the range of conditions Reynolds number $40 \leqslant Re \leqslant 140$, power-law index $0.4 \leqslant n \leqslant 1.8$ and blockage ratio 0.167, 0.25 and 0.5. They indicated wall effect leads to delay the onset of the vortex shedding for Newtonian and shear-thickening fluids; however, any consistent relationship is not specified for shear-thinning fluids. While the value of lift force is zero for the steady flow, they concluded that its instant value goes up with the Reynolds number in the unsteady flow condition for the all studied blockage ratios and power-law indexes. Besides, increasing drag coefficient with the increasing blockage ratio, they deduced that time-averaged drag coefficient increases with the increasing value of power-law index for fixed values of Reynolds number and blockage ratio. Moreover, they observed decrement of the average drag coefficient with increasing Reynolds number for constant values of the power-law index and blockage ratio. Nonetheless, the instant values of

lift force and Strouhal number (St) decrease with increasing blockage ratio.

1.2.2. Non-Isothermal Studies for Flow Around Cylinder with Polymer/Surfactant Additives

Some turbulent pipe flow experiments [39, 40] show that using polymer additives lead to reduction in friction, however the rate of heat transfer is deteriorated under their action [41, 42]. Even though for laminar flow, significant increase in the heat transfer rate is observed experimentally for non-circular ducts [43–45] without any effect on friction factor, no heat transfer enhancement is recorded for laminar circular pipe flow [1]. In the literature, some experimental and numerical studies had been carried out related to external fluid flow from a circular heated cylinder submerged in polymer/surfactant solutions to study non-Newtonian flow and heat/mass transfer properties of these structured fluids [46].

Shah *et al.* [47] conducted an experiment with carboxy- methyl cellulose (CMC) solutions with the concentrations of 0.09%, 0.22%, 0.35%, Prandtl number order of 100 and Reynolds number between 10^2 to 10^4 to investigate heat transfer from a circular cylinder to a power-law fluid. They observed that the local Nusselt number for power-law fluids with $n < 0.8$ on the cylinder surface is considerably higher than Newtonian fluid. James and Acosta [48] investigated the laminar flow of dilute polymer solutions around a circular cylinder at Reynolds numbers less than 50, and they deduced that viscoelastic effects lead to an increase in the drag coefficient and a decrease in the heat transfer for high velocities. Moreover, Ghosh *et al.* [49] conducted experiment to observe effects of concentrated polymer solutions (0.5% to 1.5%) on the heat and mass transfer in Reynolds number $0.0018 \leq Re \leq 513$, and they could not observe any asymptotic trend as distinct from study of James and Acosta [48]. Ghosh *et al.* [50] also presented correlation for the average Nusselt number in the range of conditions $0.71 \leq n \leq 1$ and $Re \leq 513$. Hoyt and Sellin [51] found experimentally that increasing concentrations of dilute polyacrylamide solution (5 to 165 ppm) decreases the heat transfer coefficient at Reynolds numbers between 4000 and 40000, but solution viscosity is also increased correspondingly. They did not observe any perceptible difference

between water and polymer solution when an increase of viscosity was taken into account.

Rao [52] carried out an experimental study about non-Newtonian flows over a heated cylinder over a range of generalized Reynolds numbers $102 < Re < 5800$, generalized Prandtl numbers $6.5 < Pr < 79$ and power-law index $0.6 < n < 1$. It was found that increasing polymer concentration of purely viscous non-Newtonian fluids causes to decrease the peripherally averaged heat transfer coefficient, and the local Nusselt number variation with the angle measured from stagnation point has only one minimum point. Besides, the new correlation of the averaged Nusselt number was proposed for purely viscous power-law fluids.

A few numerical studies [25, 53] about forced convection heat transfer from a circular cylinder to power-law fluids under unconfined condition in the steady flow regime ($Re < 40$) show that both the surface-averaged and local Nusselt numbers enhance with increasing shear-thinning behavior. In addition, decreasing value of the local Nusselt number with decreasing Prandtl number was observed.

In an extensive study, two-dimensional time dependent forced convection heat transfer in power-law fluids from a circular cylinder was studied by Patnana *et al.* [54] in the following range of conditions: Reynolds number $40 \leq Re \leq 140$, Prandtl number $1 \leq Pr \leq 100$, power-law index $0.4 \leq n \leq 1.8$. They found that irrespective of the power-law index, the averaged Nusselt number increases with Reynolds or Prandtl number. They emphasized that shear thinning fluids have higher heat transfer rates while shear thickening fluids have lower rates of heat transfer in comparison with Newtonian fluid. Dependence of the power-law index on the local and time-averaged Nusselt numbers were also plotted.

1.2.3. Proposed Mechanisms of Drag Reduction

Even though there are pretty much studies about laminar and turbulent drag reduction, the mechanism of polymer-induced drag reduction still remain uncertain.

Lumley [55] who was the first explicator of the drag reduction mechanism in 1969 suggested 'time criterion' phenomenon which says that drag reduction is strictly affiliated with relaxation time of the polymer solution. They stated drag reduction occurs in case of higher relaxation time of the polymer solution than the turbulent timescale of motion. In this case, drag reduction comes from the extensional viscosity which is enhanced greatly by 'coil-stretch' transition under the time criterion. Another theory proposed by Landahl [56] suggests that the drag reduction mechanism is based on anisotropy effects in the relation between stress and deformation fields, due to extended polymers. A third explanation was given by de Gennes [57] and Joseph [58, 59], where elastic effects play a major role in drag reduction, and the elastic effect manifests itself in polymers property of storing elastic energy, leading to the suppression of small eddies in turbulence.

There are in the literature experimental [60] and direct numerical simulation studies [61] on turbulent drag reduction supporting the theory based on the effect of increased elongational viscosity. However, the experimental observation and direct numerical simulation results given by Toonder *et al.* [62] show that drag reduction decreases with polymer flexibility and after the onset of drag reduction, elasticity has even an adverse effect. They suggest that the main factor for drag reduction by polymer additives is the anisotropic stress due to extended polymers. Direct numerical simulations for turbulent channel flow reported by Gillissen [63] compare the behavior of rigid and flexible polymers and also indicate that polymer elasticity plays a minor role in drag reduction mechanism. On the contrary, there are other experimental [64, 65] and numerical studies [66] suggesting that drag reduction for polymeric solutions arise from the elastic properties of the polymer macromolecules. Besides, it was suggested that drag reduction is rather linked with the thickened viscous layers near to the duct wall [67].

The onset criterion is predicted in the study of Min *et al.* [66], and they hypothesized that the polymer molecules absorb the turbulent kinetic energy near the wall, then transform it into elastic energy when drag reduction occurs. If the relaxation time of the polymer was long enough, this elastic energy would be raised upward by

near-wall vortical motion and dissipated into buffer or log layers; thereby, the near-wall turbulence is diminished, and thus caused to drag reduction. In spite of the fact that there are many proposed theoretical mechanisms of drag reduction by different researchers, drag reduction mechanism in the presence of polymer solutions is still nearly unknown.

1.3. Objective

Even though there are many studies about internal flow with polymer additives, shortage of polymer induced external flow studies in laminar to transition regime restrict technological advancements and applications. Therefore, unconfined laminar/transition flows over circular cylinder is considered for this study, and shear-thinning, shear-thickening and viscoelasticity impacts on laminar/transition flow is studied numerically. The basic aim of this study is a parametrical analysis and comparison of similar effects in laminar periodic vortex shedding and transition flow regimes for external flows. Therefore, two-dimensional numerical simulations are considered for unconfined non-isothermal/isothermal flow of a dilute polymer/surfactant solution over a circular cylinder. Purely shear thinning/thickening, purely elastic and combined shear thinning and elastic effects are compared in terms of the changes in various flow features such as drag and lift coefficients, vortex shedding frequency, separation point location, vortex formation length and wake region structure for periodic vortex and transition regimes, through the use of Newtonian, generalized Newtonian (power-law), Oldroyd-B, Giesekus and FENE-P constitutive models. While the power-law and Oldroyd-B models display purely shear thinning/thickening and purely elastic effects, respectively, the combined effects are monitored by the viscoelastic Giesekus and FENE-P models, which display shear rate dependent viscosity property through anisotropy and finite extensibility parameters, respectively. This study also deals with wall confinement impact on Newtonian and power-law fluids past a circular cylinders in the blockage ratio range $0.02 \leq B \leq 0.5$.

Additionally, the unconfined non-isothermal flow past a circular cylinder with both inelastic and viscoelastic non-Newtonian properties is considered to investigate

the effects of polymer/surfactant additives on forced convection heat transfer properties in terms of heat transfer enhancement or deterioration in periodic vortex shedding. The local and averaged heat transfer coefficients and temperature fields in the periodic vortex shedding regime under uniform (constant) wall temperature condition are revealed.

1.4. Outline of the Thesis

The thesis has four major chapters. After this introduction chapter with background and objective, mathematical formulation and solution method are given in Chapter 2 which gives insight about formulation of CFD simulations. In Chapter 3, results are discussed on the basis of output parameters of non-isothermal/isothermal flow calculations in detail. Finally, Chapter 4 concludes the thesis by a summary of the results and future works.

2. MATHEMATICAL FORMULATION AND SOLUTION METHOD

2.1. Domain and Geometry

In this study, cylinder with diameter D is placed symmetrically between upper and lower walls in a rectangular channel, and the cylinder is exposed to a free stream with uniform inlet velocity U. No slip condition is applied on cylinder surfaces, as well as on confining boundaries. Moreover, outlet pressure is set as 0 and uniform velocity inlet boundary condition is selected according to Reynolds number. The distances are illustrated on the Figure 2.1 are taken as $10D$ and $25D$ respectively.

For non-isothermal flow condition, uniform inlet velocity U and constant temperature $T = T_0$ are imposed at the inlet of the flow domain. No slip condition is applied for velocity on the upper and lower walls. The wall temperatures are set to $T = T_0$. On the surface of the cylinder, the no-slip condition is used, and the uniform temperature is $T = T_w$. At the outlet,the pressure and heat flux are set to zero.

Blockage ratio (B) is defined as the projected area of the object in the flow direction to the cross-sectional area of the computational domain. According to Zdravkovich [68], in order to avoid the upper and lower stationary walls effects on the unconfined flow structure near the cylinder, the blockage ratio B which is defined as D/H should not be more than 0.1, it is used as 0.02, in this study for the unconfined case. Additionally, in order to examine wall effect on Newtonian and Non-Newtonian inelastic (power-law) fluid flow around a circular cylinder, domains with different heights are used for subsequent investigations. It is also stated that for the condition of $0.1 < D/H < 0.6$, blockage considerably alters the flow [68]; therefore, the range of condition $0.02 < D/H < 0.5$ is studied for Newtonian and power-law fluids to investigate confinement effect.

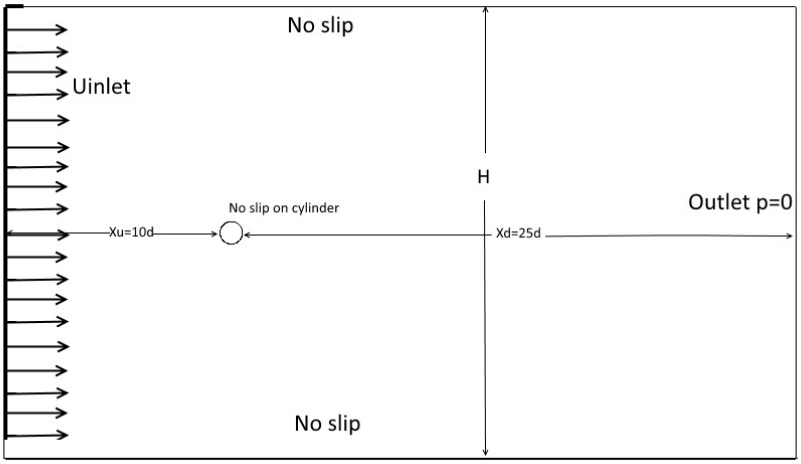

Figure 2.1. Computational domain and boundary conditions.

2.2. Governing Equations and Constitutive Models

Considering a dilute solution of a base fluid (water) with polymer/surfactant additives, the mass conservation, linear momentum and energy equations under the absence of body forces for an incompressible flow are given respectively as,

$$\nabla.\mathbf{V} = 0 \tag{2.1}$$

$$\rho\frac{D\mathbf{V}}{Dt} = -\nabla p + \nabla.\overline{\overline{T}} \tag{2.2}$$

where ρ is the fluid density, $\mathbf{V}$ is the velocity, p is pressure, t is the time and $\overline{\overline{T}}$ is the extra stress tensor. For non-isothermal flows, energy equation is defined as,

$$\rho c_p\frac{DT}{Dt} = k\nabla^2 T + r + \overline{\overline{\sigma}} : \overline{\overline{D}} \tag{2.3}$$

where c_p is the specific heat capacity, T is the temperature, r is the heat generated by the external sources which is neglected, k is the thermal conductivity, the term $\overline{\overline{\sigma}} : \overline{\overline{D}}$ represents the viscous dissipation which consists of the total (Cauchy) stress tensor

$\overline{\overline{\sigma}} = -p\overline{\overline{I}} + \overline{\overline{T}}$, and the rate of deformation tensor, $\overline{\overline{D}}$.

For Newtonian case, the stress tensor can be defined as:

$$\overline{\overline{T}} = 2\eta\overline{\overline{D}} \tag{2.4}$$

where $\overline{\overline{I}}$ is unit tensor and η is the fluid viscosity. In Power-law, or Generalized Newtonian model, the stress tensor $\overline{\overline{T}}$ in the Navier- Stokes equations becomes:

$$\overline{\overline{T}} = 2\eta(\dot{\gamma})\overline{\overline{D}} = m\dot{\gamma}^{n-1}\overline{\overline{D}} \tag{2.5}$$

where $\dot{\gamma}$ is the shear rate which is defined by $\dot{\gamma} = \sqrt{\frac{1}{2}\overline{\overline{D}} : \overline{\overline{D}}}$, m is the consistency factor, and n is the power-law index. When n equals to 1, the model represents the Newtonian and viscoelastic fluids; when n is less than 1, the fluid is shear thinning; and when n is greater than 1, the fluid is shear thickening [9].

The modified Reynolds number is defined as,

$$Re = \frac{\rho U^{2-n} D^n}{m} \tag{2.6}$$

where U is the velocity scale and D is the length scale.

The modified Prandt number (Pr) is,

$$Pr = \frac{c_p m}{k}\left(\frac{U}{D}\right)^{n-1} \tag{2.7}$$

Weissenberg number, $Wi = \lambda U/D$, is the dimensionless parameter which indicates the value of elasticity for viscoelastic fluids. It is the ratio of the elastic forces to viscous forces [69]. As it is understood from the definition of Weissenberg number, $Wi = 0$ represents purely viscous fluid while $Wi = \infty$ indicates purely elastic response.

For viscoelastic models, the extra-stress tensor is the sum of the viscoelastic component $\overline{\overline{T_1}}$ and the purely viscous component $\overline{\overline{T_2}}$ as,

$$\overline{\overline{T}} = \overline{\overline{T_1}} + \overline{\overline{T_2}} \tag{2.8}$$

Oldroyd-B model is one of the simplest differential viscoelastic model which is slightly better than Maxwell model. Implication of the purely stress component of the extra stress results in better behavior of the numerical scheme. For the Oldroyd-B Model, the viscoelastic component ($\overline{\overline{T_1}}$) is calculated as,

$$\overline{\overline{T_1}} + \lambda \overset{\nabla}{\overline{\overline{T_1}}} = 2\eta_1 \overline{\overline{D}} \tag{2.9}$$

where the symbol $\overset{\nabla}{()}$ represents the upper convected derivative, η_1 is the viscosity of the polymer/surfactant additive, and λ represents the relaxation time. The purely viscous component ($\overline{\overline{T_2}}$) is given by,

$$\overline{\overline{T_2}} = 2\eta_2 \overline{\overline{D}} \tag{2.10}$$

where $\overline{\overline{D}}$ is the rate of deformation tensor, and η_2 is the viscosity of the purely viscous part. The relation between η_1 and η_2 is expounded by β which is the viscosity ratio,

$$\beta = \frac{\eta_2}{\eta_2 + \eta_1} \tag{2.11}$$

Viscosity ratio (β) denotes the contribution of the solvent viscosity to the total solution viscosity [9].

Giesekus model is used for more realistic approach to model viscoelastic fluid. It exhibits both shear thinning and a non-quadratic first normal-stress difference at high shear rates [9].

$\overline{\overline{T_1}}$ is computed in the Giesekus model from;

$$\left(\overline{\overline{I}} + \frac{\alpha\lambda}{\eta_1}\overline{\overline{T_1}}\right).\overline{\overline{T_1}} + \lambda \overset{\nabla}{\overline{\overline{T_1}}} = 2\eta_1\overline{\overline{D}} \tag{2.12}$$

The Giesekus model contains four parameters: the dimensionless "mobility factor" α which is associated with anisotropic hydrodynamic drag and Brownian motion, the solvent and polymer contributions to the zero shear rate viscosity η_2 and η_1, a relaxation time λ. Mobility factor (α) indirectly connected with concentration of the solution as $\alpha = 0$ represents dilute solution whereas $\alpha = 0.5$ represents concentrated solution. It should be noted that, condition of $0 < \alpha < 0.5$ is required to provide realistic properties. In addition, α is also related to shear thinning character in such a way that the reduction in the shear viscosity with Weissenberg number increases when α is increased [9].

In the FENE-P model molecules are described as dumbbells, each consisting of two spheres linked together by a spring. Differently from the Maxwell model, the springs can extend within finite limits. The model predicts a realistic shear thinning of the fluid and a first normal stress difference [9], additionally, it provides a finite elongational viscosity for all magnitudes of extension rates [70].

In the FENE-P model, the viscoelastic component of the stress tensor $\overline{\overline{T_1}}$ is defined as,

$$\overline{\overline{T_1}} + \lambda\left(\frac{\overset{\nabla}{\overline{\overline{T_1}}}}{f}\right) = 2a\eta_1\left(\frac{1}{f}\right)\overline{\overline{D}} - a\eta_1\frac{D}{Dt}\left(\frac{1}{f}\right)\overline{\overline{I}} \tag{2.13}$$

where f is a function of the stress invariants which is computed from the following equation;

$$f(\overline{\overline{T_1}}) = \frac{L^2 + (\lambda/a\eta_1)Tr(\overline{\overline{T_1}})}{L^2 - 3} \tag{2.14}$$

where $a = L^2/(L^2 - 3)$ is a constant, and L is the finite extensibility parameter which is the ratio of maximum length of the polymer chain to its length at rest. When L is increased to infinity, the constant viscosity Oldroyd-B model is recovered, and the model exhibits more and more shear thinning with decrease in the finite extensibility [71, 72].

In non-isothermal calculations, the effects of small temperature difference between the cylinder surface and non-Newtonian fluid on the flow structure and heat transfer parameters are examined in detail. $\Delta T = T_w - T_0 = 2K$, is applied to provide minimum changes in the fluid properties (ρ, η, λ). The Williams-Landel-Ferry (WLF) model is used to specify temperature dependency of the physical parameters (relaxation time λ and total viscosity η) as [73],

$$\lambda(T) = \lambda(T_0) f_1(T) \tag{2.15}$$

$$\eta(T) = \eta(T_0) f_1(T) \tag{2.16}$$

where the shift factor f_1 is defined by,

$$f_1(T) = exp\left(- \frac{c_1(T - T_0)}{c_2 + (T - T_0)} \right) \tag{2.17}$$

where T_0 is a reference temperature, and the constants c_1, c_2 are chosen as $c_1 = 5$, $c_2 = 150$ which are appropriate for the temperatures far from the glass transition temperature, leading to low relaxation times [73]. In this study, a small temperature difference $(\Delta T = T_w - T_0 = 2K)$ is considered between the cylinder surface and the fluid. Figure 2.2 shows the variation of relaxation time (λ) and total viscosity (η) with temperature according to WLF model.

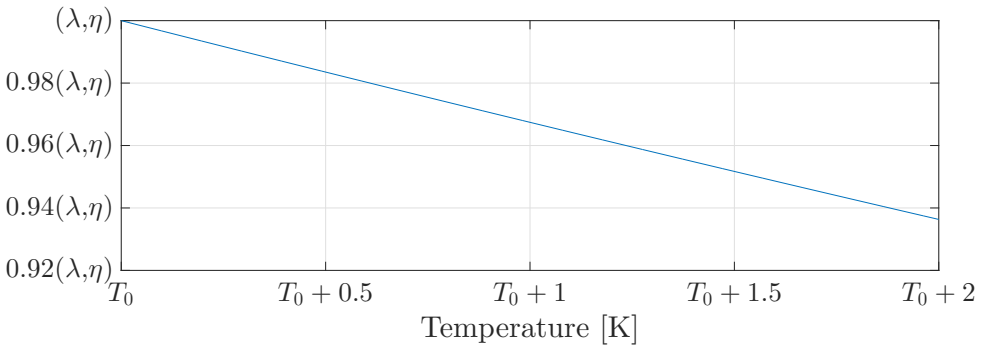

Figure 2.2. WLF function for $c_1 = 5$ and $c_2 = 150$.

The local Nusselt number $Nu(\theta)$ which changes from one point to another on the surface of the cylinder is evaluated from the temperature fields as,

$$Nu(\theta) = \frac{hD}{k} \tag{2.18}$$

where θ is the angle measured from the front stagnation point, h is the convective heat transfer coefficient which is derived from the local heat flux. Due to the periodic nature of the flow, time-averaged values of 10 to 15 settled periodic cycles are considered in the calculation of the local Nusselt number.

The overall surface averaged Nusselt number ($\overline{Nu}$) is calculated by integrating the local Nusselt number over the surface of the cylinder as,

$$\overline{Nu} = \frac{1}{2\pi} \int_0^{2\pi} Nu(\theta) d\theta \tag{2.19}$$

2.3. Solution Method

Finite Element method(FEM) based solver ANSYS Polyflow is used to calculate differential equations which are defined in the flow domain. Boundary sets are defined after dividing 2D domain into finite elements as quadrilateral or triangle grids. Internal boundaries or connectors are intersections between 2 finite elements as seen in Figure 2.3.

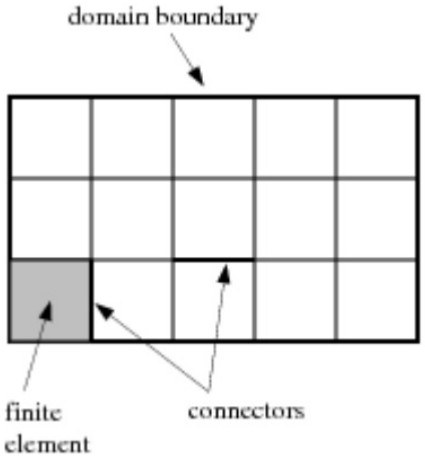

Figure 2.3. Definition of finite element [74].

Table 2.1. Mesh independency study for Newtonian fluids ($Re = 100$).

$B = 0.02$			$B = 0.05$		$B = 0.1$		$B = 0.2$		$B = 0.5$	
Grid	C_D	$\overline{Nu}$	Grid	C_D	Grid	C_D	Grid	C_D	Grid	C_D
12307	1.32	13.69	8532	1.31	11552	1.54	23092	2.09	10592	5.88
27212	1.37	13.83	26132	1.43	24302	1.62	41412	2.14	25084	5.89
52262	1.37	13.83	48334	1.44	41652	1.64	75292	2.14	36003	5.89
105252	1.38	13.82	76432	1.45	63752	1.65	104392	2.15		

For space discretization, linear interpolation for pressure and quadratic interpolation schemes for velocity and temperature variables are used. For all following calculations are carried out by using implicit Euler time integration method. EVSS interpolation is used in calculations of viscoelastic constitutive equations; however, it is not applicable to FENE-P viscoelastic model. Therefore, the DEVSS method is preferred in FENE-P calculations [74]. Typical time step for calculations is in the order of 10^{-4}. Simulations completed in 8 to 120 hours with intel i7-5930K depending upon Reynolds number and using constitutive model.

Table 2.2. Mesh independency study for shear thinning fluids ($Re = 100, n = 0.6$)

$B = 0.02$			$B = 0.05$		$B = 0.1$		$B = 0.2$		$B = 0.5$	
Grid	C_D	$\overline{Nu}$	Grid	C_D	Grid	C_D	Grid	C_D	Grid	C_D
12307	1.2	16.79	8532	1.18	11552	1.33	23092	1.71	10592	3.71
27212	1.21	16.93	26132	1.25	24302	1.39	41412	1.76	25084	3.84
52262	1.21	16.94	48334	1.25	41652	1.40	75292	1.77	36003	3.86
105252	1.21	16.93	76432	1.26	63752	1.40	104392	1.78		

Table 2.3. Mesh independency study for Oldroyd-B fluids
($B = 0.02, Re = 100, Wi = 1, \beta = 0.9$).

Grid	12554	27564	45836
C_D	1.71	1.72	1.72
$\overline{Nu}$	11.68	11.75	11.76

2.4. Mesh Independency Study and Validation

Newtonian flow at different Reynolds numbers ranging from 80 to 300 are investigated over a circular cylinder located in the above computational domain. X_u/D and X_d/D are taken as 10 and 25 respectively, and blockage ratio (D/H) is taken 0.02 for the test cases as suggested in Zdravkovich's limitation [68] as unconfined flow condition; afterwards, domains with blockage ratios 0.05, 0.1, 0.2 and 0.5 are analyzed in order to understand wall proximity effects on the flow structure and parameters.

In this study, finite-element computational fluid dynamics (CFD) program, ANSYS Polyflow, is used for simulating Newtonian and non-Newtonian flow applications. Convergence test value is set to 10^{-4}. Then computational meshes are generated by ANSYS Icem-CFD for determining finer mesh grid to get accuracy.

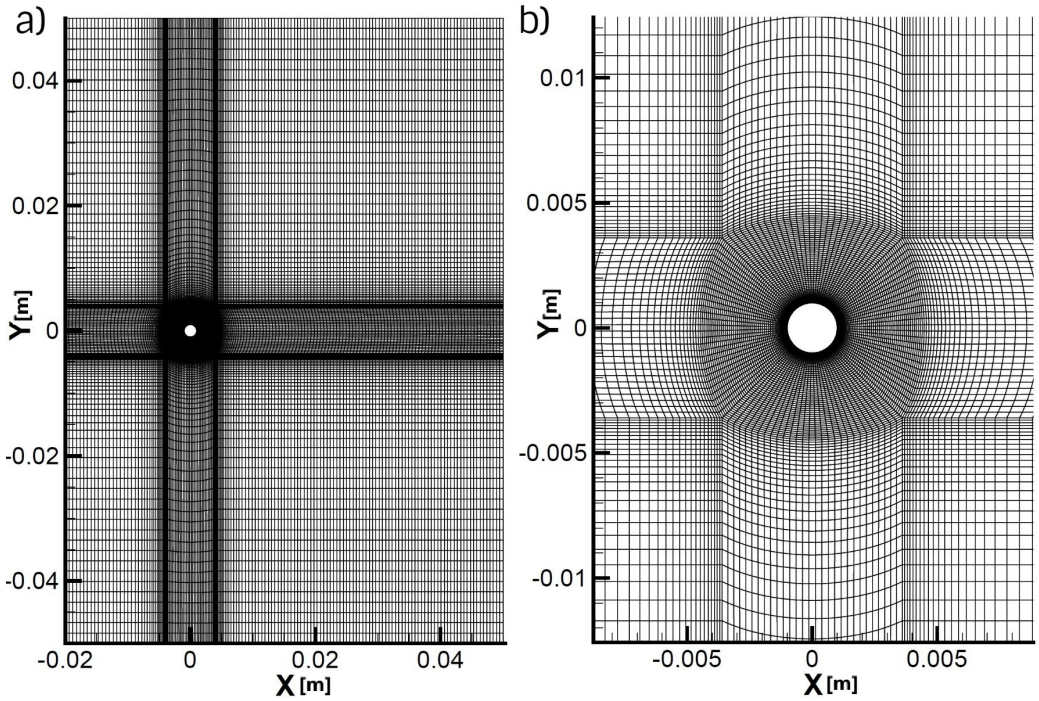

Figure 2.4. a) 27564 grid for 0.02 blockage ratio. b) Enlargement of computing mesh.

For grid independency, the computational meshes with different number of elements, generated by ANSYS Icem-CFD, are tested for the Newtonian, non-Newtonian power-law ($n = 0.6$) and Oldroyd-B ($Wi = 1$) cases at the value of the Reynolds number $Re = 100$. In Table 2.1,2.2 and 2.3 meshes with underlined grid numbers which have less than %1 difference with finest grids are found appropriate to perform analyses in terms of accuracy and computational availability. The average Nusselt number values are checked only for $B = 0.02$ as non-isothermal flow is investigated with unconfined flow condition. Apart from number of grids, some mesh criteria such as aspect ratio, skewness and smoothness are taken into consideration in mesh generation.

After mesh generation and grid independency tests (Table 2.1 and 2.2), convergence of the solutions is tested with respect to data published in the literature. Newtonian ($n = 1$) drag coefficient value for $Re = 100$, which is around 1.37, is found to be close to the experimental data values published in the literature for unconfined flow around a circular cylinder [75, 76]. Drag coefficient values calculated using the power-law model are also compared with the numerical work of Patnana *et al.* [24],

and good quantitative agreement ($C_D \approx 1.2$) is found for $n = 0.6$. Figure 2.4 shows the computational structured mesh chosen for the simulations. For non-isothermal flow, the Newtonian result for average Nusselt number ($\overline{Nu} = 13.83$) at $Re = 100, Pr = 10$ is in good agreement with the experimental correlations presented in [77,78]. The power-law ($n = 0.6$) result ($\overline{Nu} = 16.93$) is similar to the value obtained in the numerical study by Patnana *et al.* [54].

3. RESULTS AND DISCUSSION

Newtonian and inelastic (power-law), elastic (Oldroyd-B, FENE-P and Giesekus) non-Newtonian fluid models are adopted in the flow simulations. Pure shear thinning/shear thickening effects are monitored through the inelastic power-law model. The viscoelastic Oldroyd-B is a constant viscosity model, unable of predicting shear thinning, which therefore predicts purely elastic effects. This model is also derivable from a microstructural model which consists of Hookean dumbbells representing polymer molecules in a Newtonian solvent. The dumbbells are formed of two identical beads and an infinitely extensible connecting spring leading to an unbounded extensional viscosity at finite extension rates, in elongational flow regions. The combined shear thinning and weakly elastic effects for dilute polymer/surfactant solutions, are investigated through the Giesekus and FENE-P viscoelastic models. The Giesekus model includes the effects of anisotropic hydrodynamic drag and Brownian motion on polymer/surfactant molecules through the mobility factor (α) [9]. This model displays shear thinning behavior which increases with increasing α. The FENE-P model is based on finitely extensible non-linearly elastic springs connecting the beads for the dumbbell representing the polymer/surfactant molecules. The finite extensibility parameter L is the ratio of the length of a fully extended spring to its equilibrium length. When L is infinite, the Oldroyd-B model is recovered [9]. This model also displays increasing shear thinning properties with decrease in the finite extensibility parameter L. Both the Giesekus and FENE-P models lead to bounded extensional viscosities in elongational flow regions [9]. The elongational viscosity increases with decrease in the mobility factor for the Giesekus model, and with increase in the finite extensibility parameter for the FENE-P model [71].

For the two-dimensional flow simulations, the Reynolds number range is $80 \leq Re \leq 300$, which covers the laminar periodic vortex shedding and transition flow regimes. The power-law index n is chosen in the range $0.6 \leq n \leq 1.2$, to cover and compare shear thinning and shear thickening effects. For a dilute polymer/surfactant solution the viscosity ratio is fixed at $\beta = 0.9$ and weakly elastic effects are repre-

sented by the Weissenberg number in the range of $0 \leq Wi \leq 1.2$. The flow fields obtained by the simulation results are displayed and discussed in terms of the drag and lift coefficients, the vortex shedding frequency (Strouhal number) and the onset of vortex shedding, the separation angle, the vortex formation length, and the wake region streamline structure. Wall confinement effect is also investigated.

Non-isothermal simulations are carried out to reveal and compare different types of non-Newtonian effects on heat transfer characteristics for the vortex shedding flow past a cylinder due to polymer/surfactant additives. Pure shear thinning viscosity effects are monitored through the inelastic power-law model for the power-law index range $0.6 \leq n \leq 1$. The constant viscosity Oldroyd-B model is used to reveal the effects of pure viscoelasticity on heat transfer properties. The combined elasticity and shear thinning effects are reflected by the Giesekus and FENE-P models through the mobility factor α and the finite extensibility parameter L, respectively. In non-isothermal flow calculations, the Weissenberg number is fixed at $Wi = 1$ in consideration of a weakly elastic dilute solution for viscoelastic models. The Prandtl number is fixed at $Pr = 10$.

3.1. Isothermal Flow Calculations

3.1.1. Drag and Lift Coefficients

Different methods for drag calculation have been used in order to obtain similar values with experimental studies in the literature.

Firstly, drag and lift coefficients are calculated by using conventional method which are defined as in Equations 3.1 and 3.2.

$$C_D = \frac{2F_D}{\rho U^2 D} \tag{3.1}$$

$$C_L = \frac{2F_L}{\rho U^2 D} \tag{3.2}$$

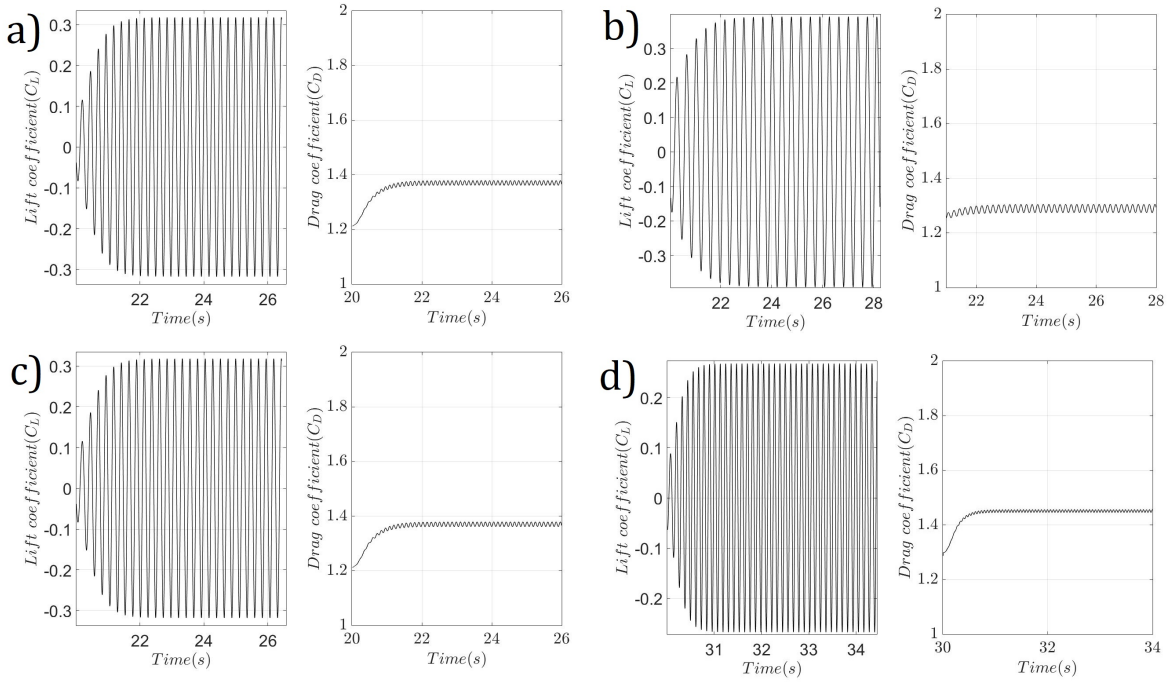

Figure 3.1. Evolution of lift and drag coefficients at $Re = 100$ for Newtonian and power-law fluid a) $n = 1$ b) $n = 0.8$ c) $n = 0.6$ d) $n = 1.2$

where F_D and F_L are the total drag and lift forces acting on the cylinder per unit length, respectively.

Figs. 3.1a-3.1d show the time-variation of lift and drag coefficients for Newtonian and non-Newtonian power-law fluid flows at $Re = 100$. After an initial period, the values of the coefficients settle into periodic oscillations. The time averaged drag coefficients and the root-mean-square (rms) values of lift coefficients are evaluated from after 10 to 15 steady periodic cycles.

Experiments and 2D numerical studies in Figure 3.2 [79, 80] showed that rms of lift increases up to Reynolds number $Re = 300$ (with a value of $C_L \approx 0.6$ for $Re = 300$) for Newtonian flow, and these values and trends are matched with results of the present study which are showed in Figure 3.3a. The values of the lift coefficient also increase with increasing Reynolds number for the power-law shear thinning and shear thickening fluids. It can also be observed in Figure 3.3a that the lift coefficient

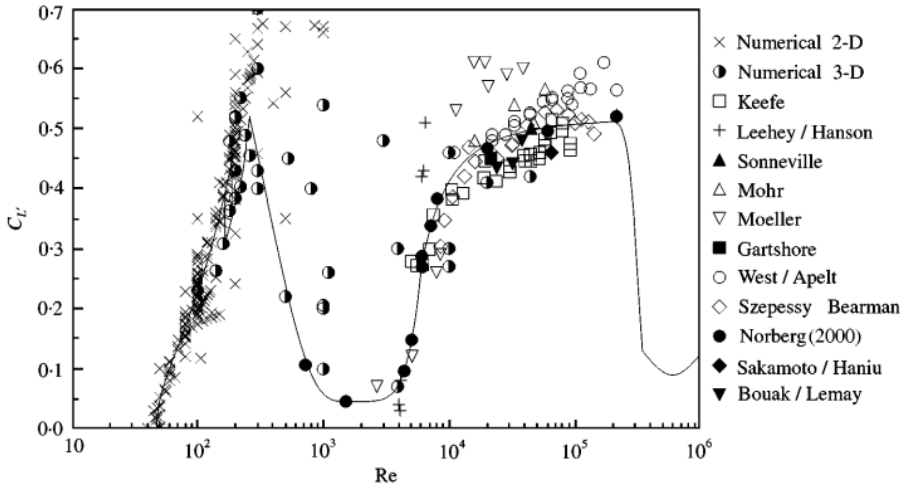

Figure 3.2. C_{Lrms} vs Reynolds number (Re) in literature [79].

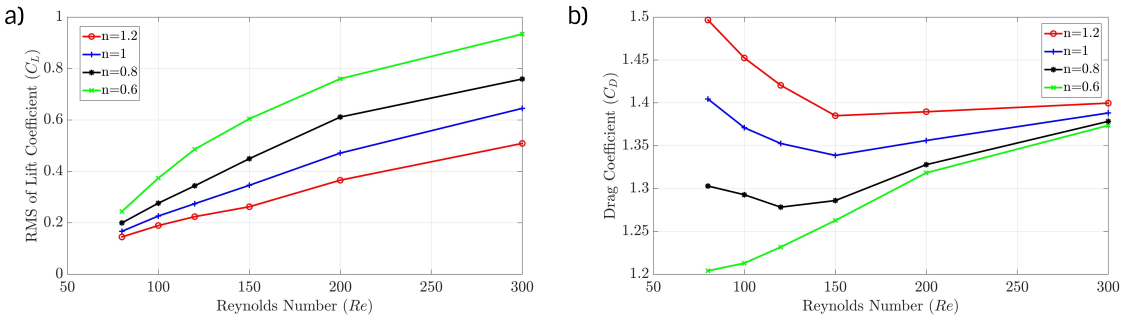

Figure 3.3. a) Variation of rms values of lift coefficient with Reynolds number for different power-law indeces b) Variation of time-averaged drag coefficient with Reynolds number for different power-law indeces

increases with increasing power-law index at a fixed Reynolds number. These trends for power-law fluids were also observed in previous numerical study in the literature for the Reynolds number range $40 \leq Re \leq 140$ in the case of unconfined flow past a circular cylinder [24].

The predicted drag coefficient values for Newtonian fluids shown in Figure 3.3b are in agreement with Wieselsberger's experimental data [75]. It can also be observed that shear thickening increases the drag coefficient while shear thinning decreases it up to $Re = 300$. This trend can also be found in the study Patnana *et al.* [24] for

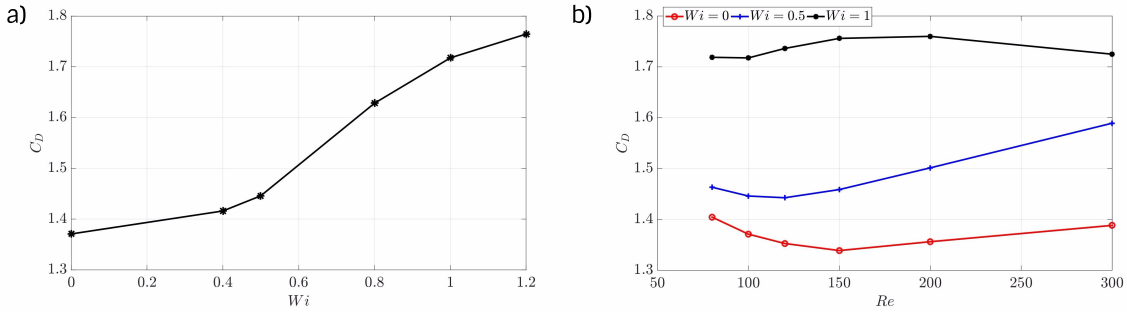

Figure 3.4. a) Effect of viscoelasticity on time averaged drag coeffcient ($Re = 100$, $B = 0.02$) b) Time averaged drag coeffcient variation of Oldroyd-B fluids with Reynolds number

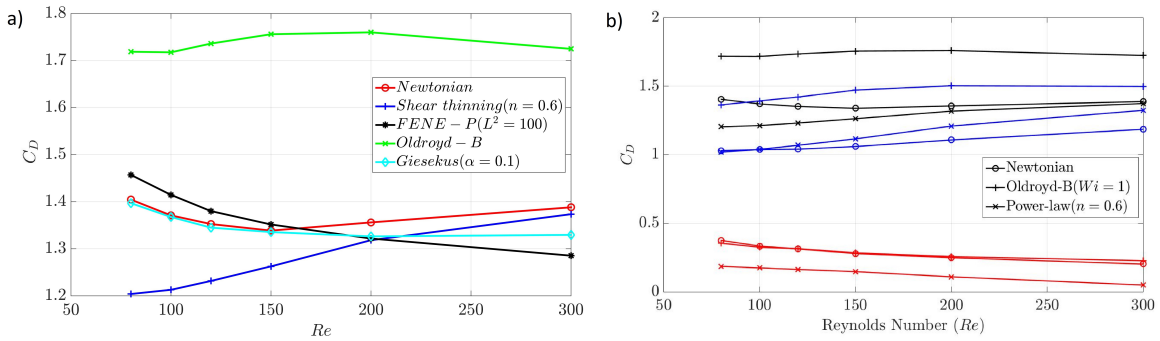

Figure 3.5. a) Time averaged drag coefficient variation with Reynolds number for different models b) Red: Friction component of drag coefficient (C_{Df}), blue: Pressure component of drag coefficient (C_{Dp}), black: Total drag coefficient (C_D)

the Reynolds number range of $40 \leq Re \leq 140$. Drag reduction is expected for shear-thinning fluids due to reduction in viscosity with increasing shear rate in the boundary layer regions close to the cylinder's wall. Moreover, shear thinning effect reduces with increasing the Reynolds number number, i.e. the change in the power-law index has smaller effect on drag coefficient in the transition regime.

Figure 3.4a presents the variation of the drag coefficient under elastic effects for the Oldroyd-B fluid at $Re = 100$, and in the range of $0 \leq Wi \leq 1.2$. From Figure 3.4a it can be deduced that the drag coefficient increases with increasing elasticity at constant Reynolds number ($Re = 100$). In Figure 3.4b, the behavior of the drag

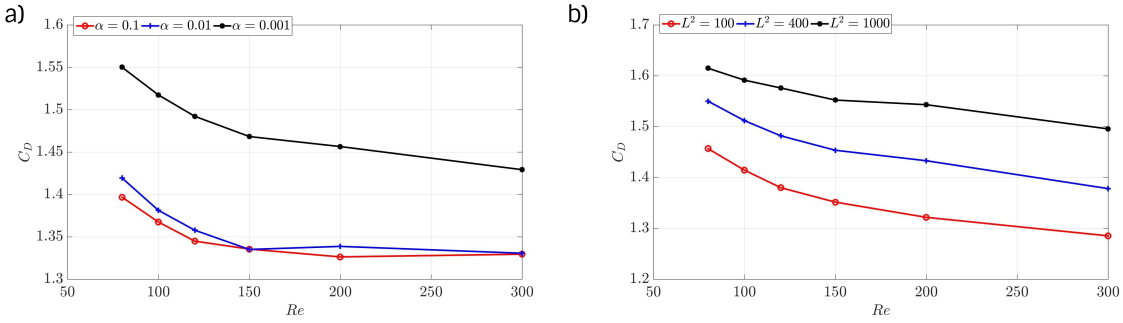

Figure 3.6. a) Effect of mobility factor on the time averaged drag coefficient for Giesekus fluid at $Wi = 1$ b) Effect of extensibility parameter on the time averaged drag coefficient for FENE-P fluid at $Wi = 1$

coefficient is displayed and compared for the Newtonian ($Wi = 0$) and the Oldroyd-B ($Wi = 0.5$ and $Wi = 1$) fluids in the Reynolds number range of $80 < Re < 300$. Elastic effects lead to increase in drag with respect to Newtonian case for the entire range of periodic vortex shedding and transition regimes, as observed in Figure 3.4b.

In Figure 3.5a the drag coefficient trends are compared for Newtonian and non-Newtonian inelastic power-law and elastic Oldroyd-B, Giesekus and FENE-P models in the periodic vortex shedding and transition flow regimes. The viscosity ratio and the elasticity parameters are fixed. The power-law index, the mobility factor and the finite extensibility parameters are chosen from typical values for a dilute solution. It may be observed that the constant viscosity Oldroyd-B fluid predicts a much higher drag coefficient than the Newtonian and other non-Newtonian models. Higher shear thinning in the power-law model ($n = 0.6$) leads to drag reduction compared to Newtonian fluid in the periodic vortex shedding, however with a decrease in reduction for higher Reynolds numbers. The Giesekus and FENE-P models predict much lower drag coefficients compared to Oldroyd-B fluid due to effective shear thinning, although there is no significant difference in the trend and the values compared to Newtonian case in the periodic regime. However these models exhibit some drag reduction in the transition flow, compared to Newtonian fluid.

In Figure 3.5b the variations in the pressure (form) drag (C_{Dp}) and the friction (viscous) drag (C_{Df}) coefficients are displayed to observe separately their contributions to the total drag, for the Newtonian, power-law shear thinning ($n = 0.6$) and the Oldroyd-B ($Wi = 1$) fluids. The shear thinning fluid has the lowest friction drag and the elastic fluid has the highest pressure drag contributions. It may be deduced that total drag reduction due to shear thinning is due to reduction in friction drag as a result of decrease in apparent viscosity in the boundary layer where velocity gradients are higher. Also, the increase in drag for the elastic fluid may be associated with the increase in pressure (form) drag, which can also be confirmed by the change of the flow separation point location, as will be shown in the subsection 3.1.3.

Effects of the mobility factor (α) for the Giesekus model and the extensibility parameter (L) for the FENE-P model on the drag coefficient are demonstrated in Figure 3.6a and Figure 3.6b respectively at Weissenberg number $Wi = 1$ and Reynolds number $Re = 100$. The drag coefficient is observed to decrease with increasing mobility factor (α) at constant elasticity in the Giesekus model due to anisotropic effects leading to shear thinning, as seen in Figure 3.6a. It can also be deduced from Figure 3.6b that increasing the extensibility parameter (L) in the FENE-P model at constant elasticity ($Wi = 1$) increases the drag coefficient. As it has been mentioned before, the increase in finite extensibility leads to a reduction in shear thinning behavior. Therefore, the increase in the anisotropy parameter in the Giesekus model, and the decrease in the finite extensibility parameter in the FENE-P model leading to shear thinning reduce the drag coefficient in periodic vortex shedding.

Unlike conventional drag coefficient calculation (Equation 3.1), Rajagopalan and Antonia [81] suggested that Reynolds normal stresses could be negligible at 30 diameters behind a circular cylinder. F is kinematic streamwise force component per unit length of the cylinder calculated by,

$$F = \int_{-\infty}^{\infty} [U(U - U_\infty) + (\overline{u^2} - \overline{v^2})]dy \tag{3.3}$$

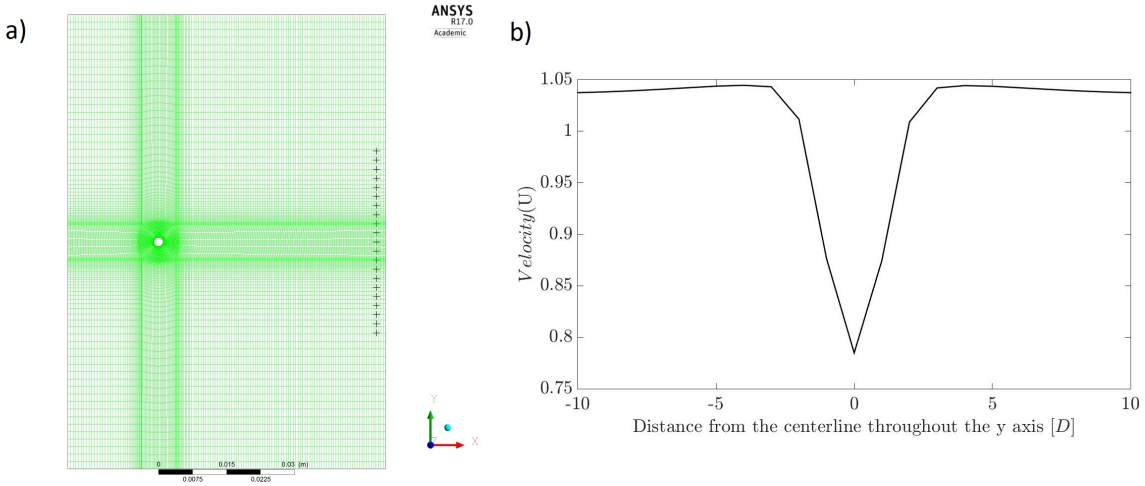

Figure 3.7. a) Mesh and 21 points ($10D$ to $-10D$) at $24D$ away from cylinder ($B = 0.02$) b) Time-averaged U velocity variation throughout the y axis at $24D$ away from the cylinder for $Re = 100$.

where U is the local mean velocity, U_∞ is the freestream velocity, u is the longitudinal velocity fluctuation and v is the lateral velocity fluctuation.

Consequently, the drag calculation turns into;

$$C_D = \underbrace{2\int_{-\infty}^{\infty}[\frac{U}{U_\infty}(1-\frac{U}{U_\infty})]d(\frac{y}{D})}_{I_1} + \underbrace{2\int_{-\infty}^{\infty}[\frac{\overline{u'^2}-\overline{v'^2}}{U_\infty^2}]d(\frac{y}{D})}_{I_2} \tag{3.4}$$

According to suggestion of Rajagopalan and Antonia [81] if the velocity profiles are taken 30 diameters away from the cylinder, the contribution of the second term can be neglected.

Figure 3.7a shows the domain which is used in calculation of drag coefficient (Equation 3.4); The shown 21 points are considered at $24D$ away from the cylinder to apply the above formula of Rajagopalan and Antonia [81]. Time-averaged x velocity is plotted at that distance throughout the y axis ($10D$ to $-10D$) as seen in Figure 3.7b. In Table 3.1, results for the drag coefficient calculation with the Equation 3.4

Table 3.1. Drag calculation results of Equation 3.4 with I_1 and I_2 contributions ($24D$ away).

	$B = 0.02$			$B = 0.05$		
	I_1	I_2	C_D	I_1	I_2	C_D
$Re = 80$	1.21	0.17	1.38	1.37	0.12	1.49
$Re = 100$	1.25	0.16	1.41	1.37	0.16	1.53
$Re = 120$	1.24	0.17	1.41	1.34	0.16	1.50
$Re = 150$	1.20	0.19	1.39	1.29	0.18	1.48
$Re = 200$	1.22	0.30	1.52	1.36	0.35	1.71
$Re = 300$	1.15	0.32	1.47	1.23	0.37	1.60

Table 3.2. Drag calculation results of Equation 3.4 by using points in the vicinity of the cylinder ($B = 0.02$).

	$U_\infty = U_{max}$			$U_\infty = U_{4.point}$			
	I_1	I_2	C_D	I_1	I_2	C_D	$C_{D\,Eq.3.1}$
$Re = 80$	1.28	0.26	1.54	1.16	0.26	1.42	1.40
$Re = 100$	1.25	0.36	1.61	1.04	0.37	1.41	1.37
$Re = 120$	1.26	0.41	1.67	0.94	0.42	1.36	1.35
$Re = 150$	1.14	0.53	1.67	0.84	0.54	1.38	1.34
$Re = 200$	1.11	0.71	1.82	0.65	0.73	1.38	1.36
$Re = 300$	1.04	0.91	1.95	0.74	0.93	1.67	1.39

is given for two different blockage ratios. Due to increasing I_2 integral contribution with increasing Reynolds number, these result could not be validated with the existing literature [75].

Moreover, Son and Cetiner [82] recommended that using the velocity profiles at the location where the centerline velocity reaches 0.5 U_∞ (half of the freestream velocity) could be applicable for maximum drag coefficient calculation. These both experimental methods are checked numerically in order to get consistent results with the

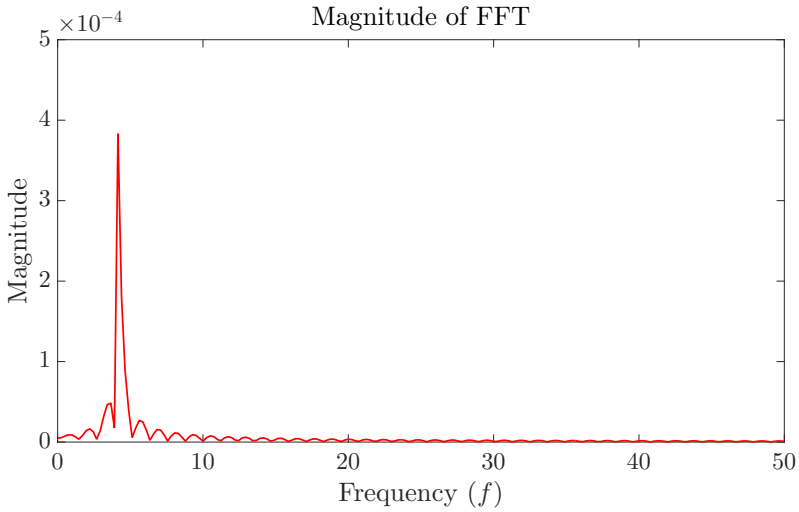

Figure 3.8. FFT spectra of the Newtonian fluid with $Re = 100$ and $B = 0.02$.

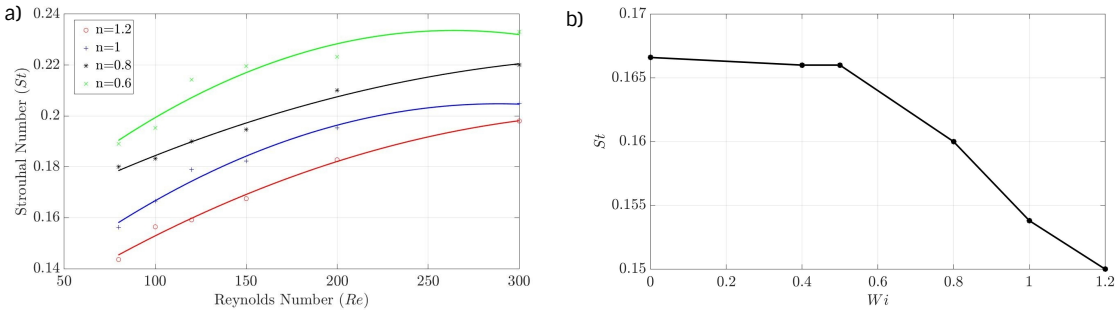

Figure 3.9. a) Shear thinning and shear thickening effect on Strouhal number b) Effect of viscoelasticity on Strouhal number ($Re = 100, B = 0.02$)

literature. In Equation 3.3, freestream velocity cannot be determined properly; therefore, velocities at points which have maximum x velocity and locate at the 4th point from centerline (Table 3.2) are assumed as freestream velocities individually. Even though calculated results are not consistent with existing literature in terms of I_2 integral contribution, drag coefficient are merely acceptable for the results with freestream velocities are taken as the velocity of 4th point from centerline at low Reynolds numbers.

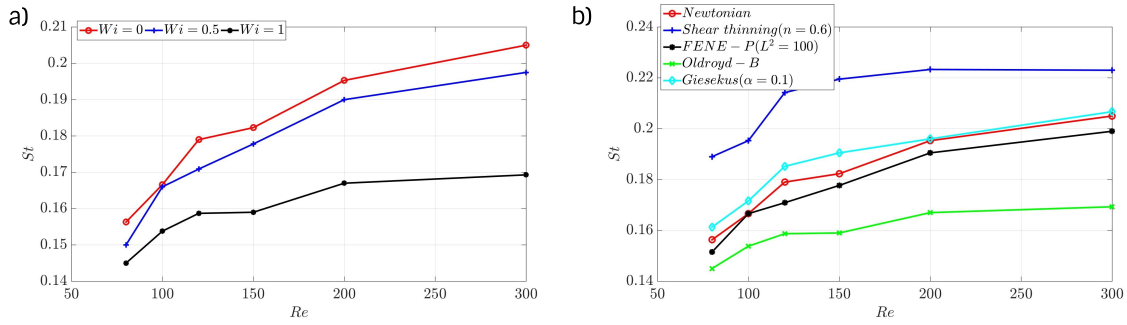

Figure 3.10. a) Strouhal number variation of Oldroyd-B fluids with Reynolds number. b) Strouhal Number variation of different models with Reynolds number.

3.1.2. Vortex Shedding and Strouhal Number

The Strouhal number represents the dimensionless frequency of vortex shedding in the periodic regime, and is defined as,

$$St = \frac{fD}{U} \tag{3.5}$$

where the vortex shedding frequency (f) is derived from Fast Fourier Transform (FFT) applied on the time evolution of the lift coefficient in all flow simulation cases, as shown in Figure 3.8. The variation of the Strouhal number with power-law index and Reynolds number is plotted in Figure 3.9a. The results for the Newtonian fluid ($n = 1$) follows the well known experimental findings in the literature [79,83]. Strouhal number is observed to decrease under shear thickening and increase under shear thinning, in accordance with the experimental observations for dilute polymer solutions by Kalashnikov and Kudin [10] and by Coelho and Pinho [18], where this increase was attributed to the reduction of the boundary layer thickness and diffusion length. For both shear thinning and thickening the Strouhal number increases with Reynolds number up to $Re = 300$.

Elasticity in the absence of shear thinning leads to a decrease in Strouhal number when the Weissenberg number increases for the Oldroyd-B fluid as it can be observed in Figure 3.9b. The variation of the Strouhal number with the Reynolds number in periodic and transition regimes is given in Figure 3.10a for Oldroyd-B fluids ($Wi = 0.5$

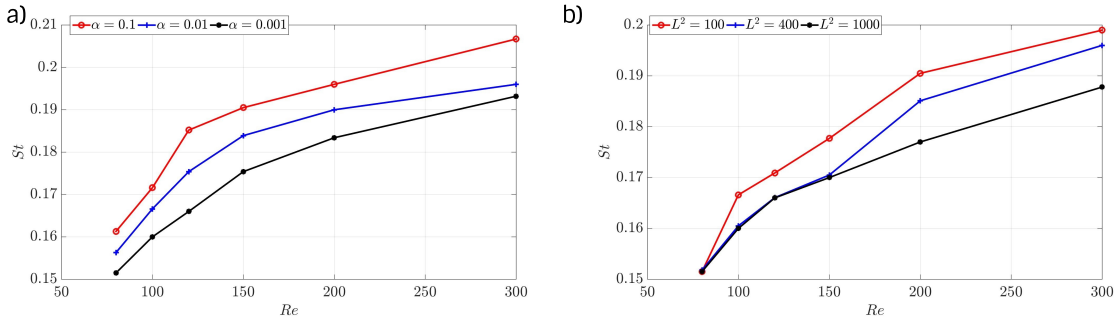

Figure 3.11. a) Effect of mobility factor on Strouhal number (St) for Giesekus fluid. b) Effect of extensibility factor on Strouhal number (St) for FENE-P fluid.

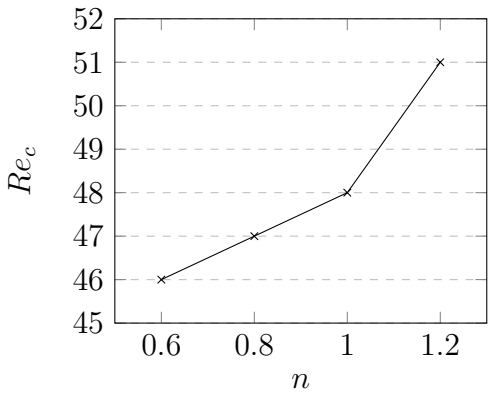

Figure 3.12. Critical Reynolds number for the onset of vortex shedding variation with power-law index (n).

and $Wi = 1$). The decrease in shedding frequency with respect to Newtonian case becomes more pronounced at higher elasticity and higher Reynolds numbers in parallel with the observations in the literature [11, 35].

It is empirically known from past studies in the literature that for geometrically similar objects, Strouhal number changes inversely with the drag coefficient for Newtonian fluids in laminar vortex shedding [84]. This relation has also been observed experimentally for polymer solutions [11]. This behavior is confirmed in Figures 3.3b-3.9a and in Figures 3.4a- 3.9b for both the inelastic shear thinning and constant viscosity elastic fluids, where decrease in drag and increase in shedding frequency with respect to Newtonian fluid are observed under shear thinning, and increase in drag and decrease in the frequency are observed under elasticity.

In Figure 3.10b the Strouhal number variations are shown for Newtonian and non-Newtonian inelastic power-law and elastic Oldroyd-B, Giesekus and FENE-P models in the periodic vortex shedding and transition regimes. The constant viscosity Oldroyd-B fluid predicts a much lower shedding frequency compared to Newtonian and other non-Newtonian models, due to purely elastic effects. Pure shear thinning effects for the power-law model ($n = 0.6$) lead to highest Strouhal numbers. The Giesekus and FENE-P viscoelastic models predict higher frequencies compared to Oldroyd-B fluid due to effective shear thinning. These results also confirm the inverse relation between the changes in the drag coefficient and the Strouhal number when compared with the trends for the drag coefficient, as observed in Figure 3.3b.

In Figure 3.11, the effects of the mobility factor (α) for the Giesekus model and the extensibility parameter (L) for the FENE-P model on the Strouhal number are shown for Weissenberg number $Wi = 1$ and Reynolds number $Re = 100$. At constant elasticity ($Wi = 1$), the Strouhal number increases with the mobility factor in the Giesekus model, as seen in Figure 3.11a, and increasing the extensibility parameter (L) in the FENE-P model decreases the Strouhal number, as seen in Figure 3.11b. These results confirm that shear thinning effects present in Giesekus and FENE-P models are responsible for the increase in vortex shedding frequency, compared to purely elastic case.

For Newtonian fluids, it is well known in the literature [76, 85] that beyond the critical Reynolds Number around $Re = 50$, the steady vortex flow in the wake becomes unsteady at the onset of periodic vortex shedding flow regime. Norberg [85] observed experimentally that critical Reynolds number for the onset of vortex shedding is nearly constant at $Re = 47.4$ for Newtonian fluids and unconfined flow around cylinders with aspect ratio (ratio of cylinder length to cylinder diameter) larger than 40. He also indicated that this onset may be delayed as the aspect ratio decreases.

The critical Reynolds number for the onset of vortex shedding is determined from the settling of periodic oscillations in the time evolution of the lift coefficient. It is found that this critical Reynolds number is nearly between $Re = 47$ and $Re = 48$

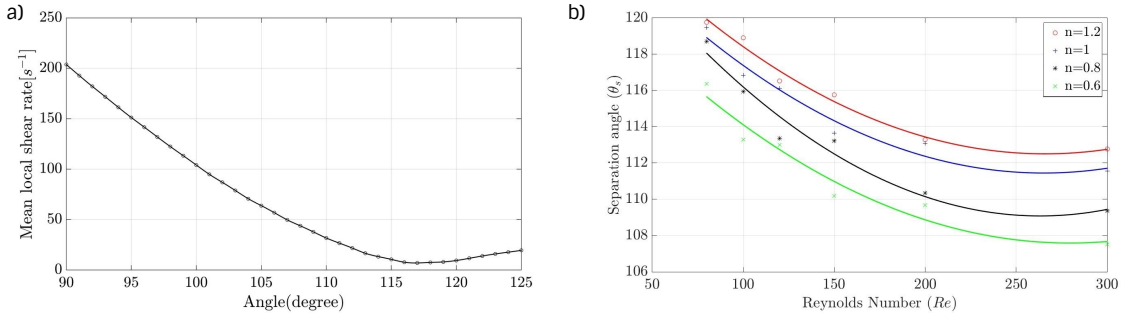

Figure 3.13. a) Mean local shear rate variation on the cylinder's top surface. b) Shear thinning and shear thickening effect on separation angle.

for the Newtonian case, which is in good agreement with experimental studies in the literature [85, 86].

In addition, it can be seen in Figure 3.12 that the critical Reynolds number for the onset of vortex shedding (Re_c) decreases under shear-thinning, while this onset is delayed for shear-thickening fluids. Even though this trend is in good agreement with the study of Rao *et al.* [38], the numerical study of Sivakumar *et al.* [26] predicts a decrease in the critical Reynolds number under shear thickening. In another numerical study, Lashgari *et al.* [87] also observed a decreasing trend for Re_c with increased shear-thinning using the inelastic Carreau model. It is also observed that weak elasticity has no significant effect on the onset of laminar vortex shedding for the Oldroyd-B fluid in the range of $0 \leq Wi \leq 1.2$. This observation is in agreement with the experimental study of Coelho and Pinho [17] which revealed that weakly elastic tylose solution has almost the same Re_c with Newtonian fluids although they measured lower Re_c values for more elastic CMC solutions.

3.1.3. Separation Angle

The flow separation point location is also investigated in the periodic vortex and transition regimes for Reynolds number up to $Re = 300$ for different flow cases. As seen in Figure 3.13a, the point at which the minimum value of time-averaged (mean) local shear stress is located on the cylinder surface is determined as the separation

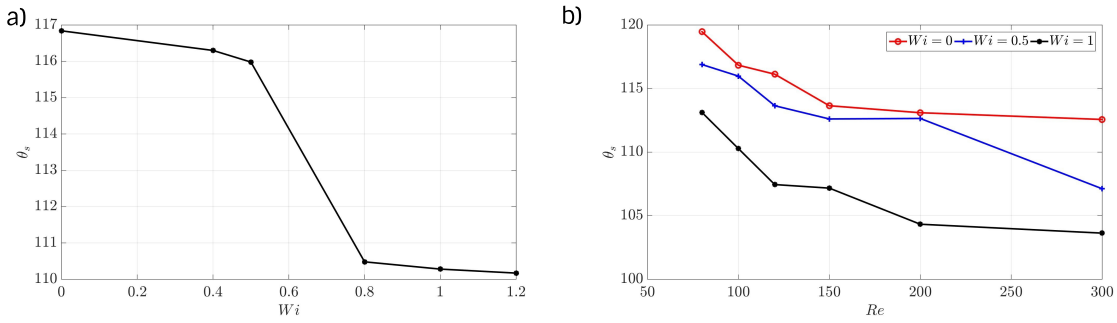

Figure 3.14. a) Effect of viscoelasticity on separation angle ($Re = 100$) b) Separation angle variation of Oldroyd-B fluids with Reynolds number.

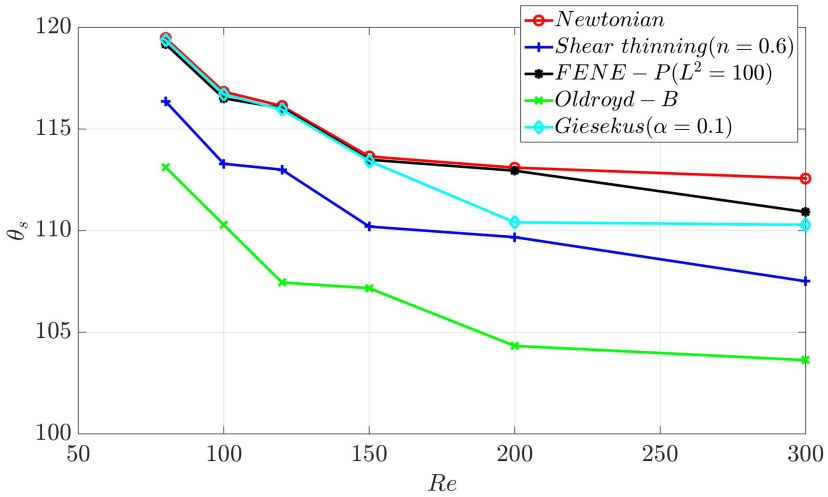

Figure 3.15. Separation angle variation of different models with Reynolds number.

point. The separation angle, denoted as θ_s, is the angle between the front stagnation point and separation point.

Figure 3.13b shows that the separation angle decreases with increasing Reynolds number for fixed power-law index; however, it also decreases under shear thinning for fixed values of Reynolds number. Good agreement is found between the results of the present study (Figure 3.13b) and data from other experimental observations and numerical studies which show a decrease from around $\theta_s = 120°$ to $\theta_s = 110°$ for Newtonian fluids [88, 89] and shear thinning polymeric solutions [19] in the range of $80 \leq Re \leq 300$.

Figs. 3.14a shows that purely elastic effects lead to a decrease in the separation angle, for the constant viscosity Oldroyd-B fluid at $Re = 100$. Figure 3.14b displays the decreasing trend of the separation angle with Reynolds number in the periodic and transition flow regimes, for different Weissenberg numbers ($Wi = 0.5$ and $Wi = 1$). Therefore, the separation point moves towards the front of the cylinder under elasticity, which would lead to an increase in the vortex formation length, as will be shown in the next subsection.

Comparison of different non-Newtonian inelastic and elastic models for θ_s, given in Figure 3.15 demonstrates that both shear thinning and elasticity reduce the separation angle. This reduction implies an increase in the pressure (form) drag coefficient with respect to Newtonian case, which was observed in Figure 3.5b. Even though the separation angle values for purely shear thinning fluids are much lower than Newtonian fluid, leading to higher pressure drag contributions, considerable decrease in the friction drag component accounts for the overall drag reduction.

3.1.4. Vortex Formation Length

In the literature, there are several definitions [15] of the vortex formation length (L_f). In this study, the vortex formation length is taken as the distance between the cylinder surface and the point with zero velocity at the centerline in the downstream region.

In Figure 3.16a, the vortex formation length can be estimated from the length between the rear stagnation point on the cylinder surface (the origin point), and the location point with zero velocity component in the streamwise direction for the Newtonian case at $Re = 100$.

The computed values of vortex formation length for Newtonian and power-law fluids can be observed in the normalized vortex formation length (L_f/D) versus Reynolds number (Re) plot in Figure 3.16b. Increasing the Reynolds number gives rise to a decrease in the formation length for all power-law indices at Reynolds numbers ranged

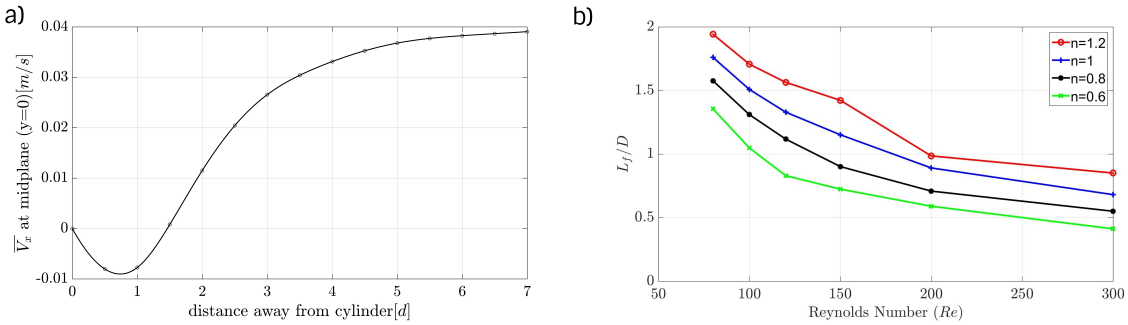

Figure 3.16. a) Time-averaged axial velocity values in the wake region throughout centerline (Newtonian fluid, $Re = 100$). b) Shear thinning and shear thickening effect on normalized vortex formation length.

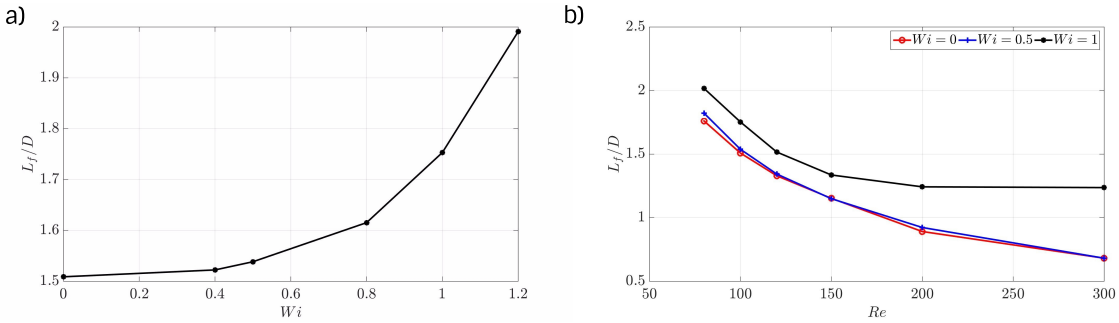

Figure 3.17. a) Effect of viscoelasticity on normalized vortex formation length ($Re = 100$, $B = 0.02$). b) Normalized vortex formation length variation of Oldroyd-B fluids with Reynolds number.

from $Re = 80$ to $Re = 300$. The Newtonian trend is similar to experimental results in Gerrard's study [83]. Figure 3.16b also indicates that for a fixed value of the Reynolds number, the vortex formation length decreases under shear thinning.

Variation of normalized vortex formation length with increasing Weissenberg number at $Re = 100$ is illustrated in Figure 3.17a. The variation with the Reynolds number at different elasticities ($Wi = 0.5$ and $Wi = 1$) is shown in Figure 3.17b. It can be observed that the vortex formation length increases with elasticity.

Therefore, the vortex formation length and shedding frequency change inversely under inelastic and elastic non-Newtonian effects, in parallel with experimental obser-

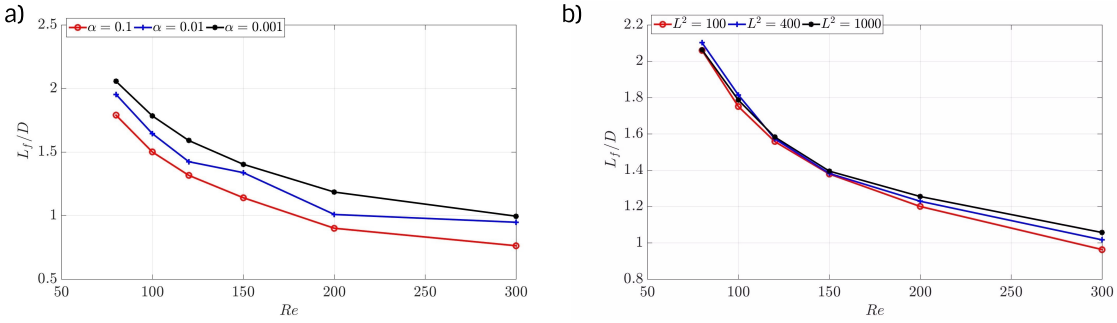

Figure 3.18. a) Effect of mobility factor on normalized vortex formation length (L_f/D) for Giesekus fluid at $Wi = 1$. b) Effect of extensibility parameter on normalized vortex formation length (L_f/D) for FENE-P fluid at $Wi = 1$.

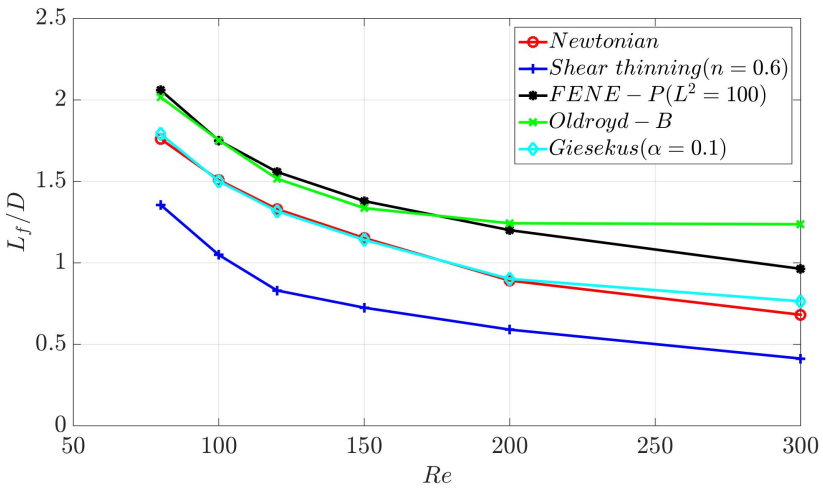

Figure 3.19. Normalized vortex formation length variation with Reynolds number for different models.

vations in the literature for Newtonian fluids [90].

In Figure 3.18a, the normalized vortex formation length decreases with increasing the mobility factor α for Giesekus fluid at a given Reynolds number and at constant elasticity $Wi = 1$. As seen in Figure 3.18b, increasing the finite extensibility parameter in the FENE-P model ($Wi = 1$) slightly increases the normalized vortex formation length at a given Reynolds number. These results are related to shear thinning effects observed with the increase in the mobility factor for the Giesekus model and the decrease in the extensibility parameter for the FENE-P model.

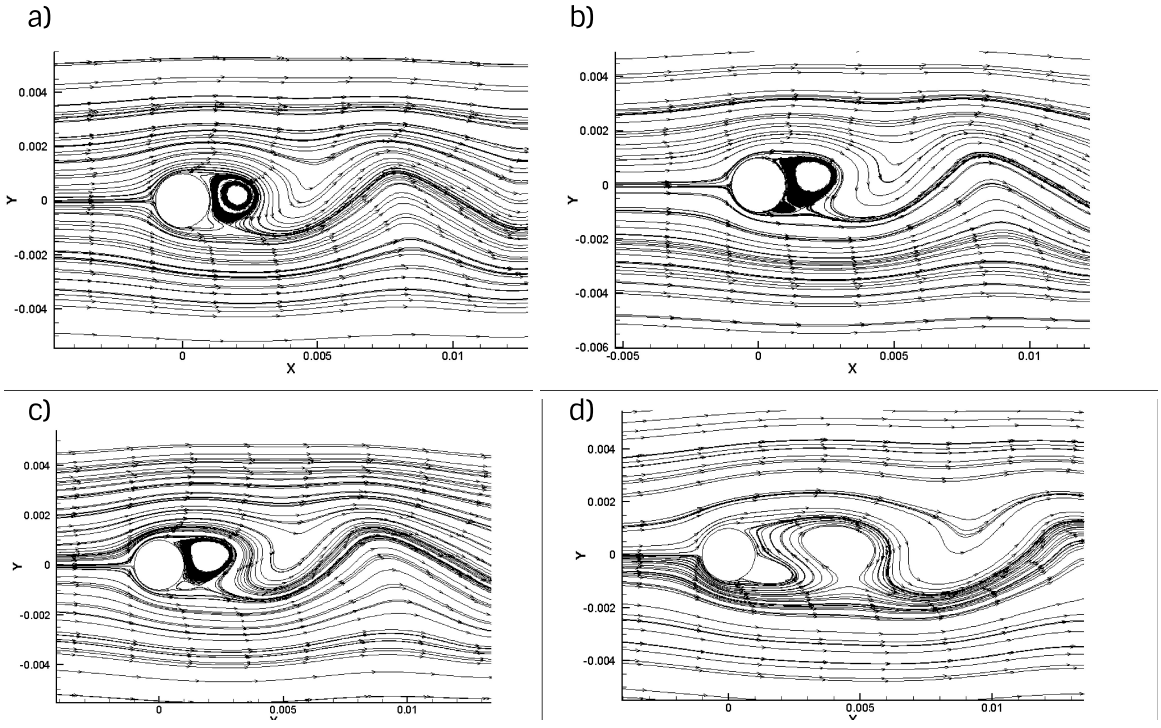

Figure 3.20. Streamlines in the vicinity of the cylinder for Newtonian fluid with $B = 0.02$ and $Re = 100$ a) $n = 0.6$ b) $n = 0.8$ c) $n = 1$ d) $n = 1.2$

The normalized vortex formation length variations in the periodic shedding and transition regimes, are given in Figure 3.19 for the considered inelastic and elastic models. The trends for the Giesekus and FENE-P models ($Wi = 1$) reflecting combined shear thinning and elastic effects, are between the trends of purely shear thinning (power-law, $n = 0.6$) and purely elastic (constant viscosity Oldroyd-B, $Wi = 1$) cases, as expected.

Streamlines in the wake region of the cylinder for Reynolds number $Re = 100$ and power-law index from $n = 0.6$ to $n = 1.2$ are presented in Figure 3.20a-3.20d. The streamlines are plotted at the time when the lift coefficient reaches the peak value of steady periodic oscillations for each case. It is revealed that both the vortex formation length and the width of the wake region increase from shear-thinning ($n < 1$) to shear-thickening ($n > 1$) cases. Figure 3.21a-3.21d shows that elasticity also increases the vortex formation length and the wake width, for the Oldroyd-B fluid at $Re = 100$.

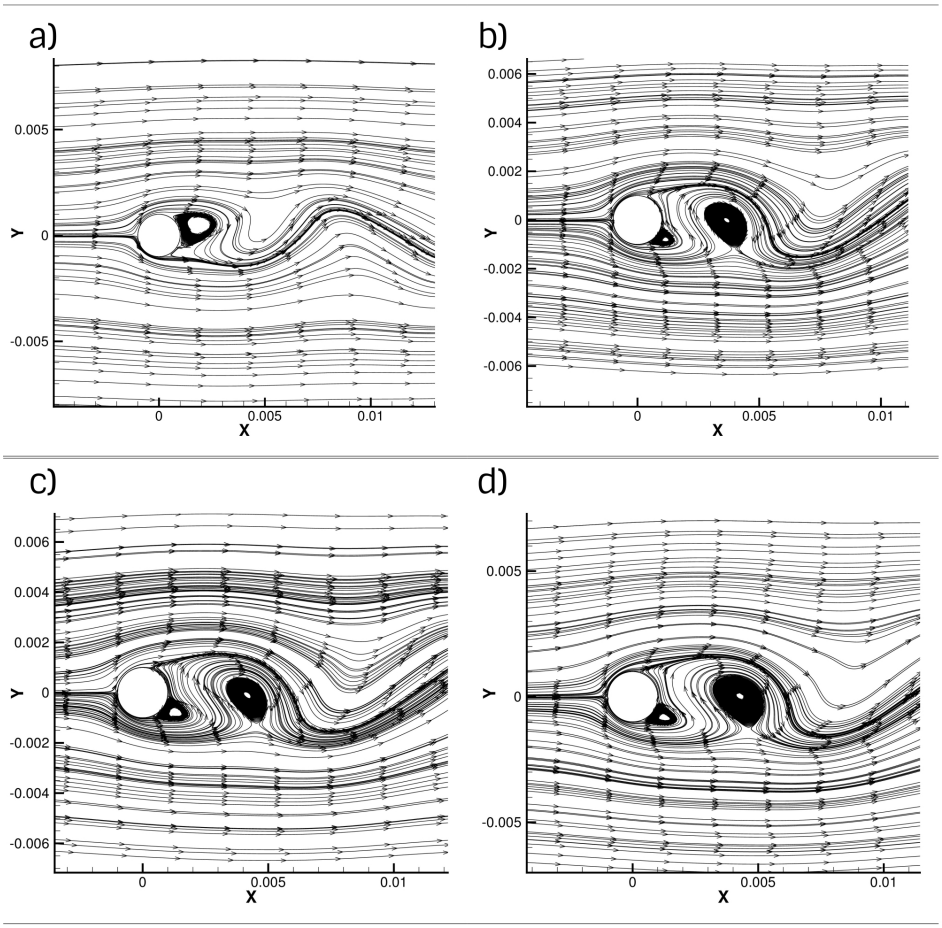

Figure 3.21. Streamlines in the vicinity of the cylinder for Oldroyd-B fluid at $Re = 100$ a) $Wi = 0.4$ b) $Wi = 0.8$ c) $Wi = 1$ d) $Wi = 1.2$

3.1.5. Blockage Effect and Wall Proximity

In the literature [68], it is stated that the blockage effect can be negligible for the cases of $B < 0.1$, and for $0.1 < B < 0.6$ cases, blockage impacts the flow considerably, so correction of the measured date is required. For the case of $B = 0.6$ and above, correction is meaningless because of excessive impact of blockage on the flow around a cylinder.

In this study, 4 different blockage ratios are investigated in order to analyse blockage effect on the purely inelastic and viscous flow around a cylinder.

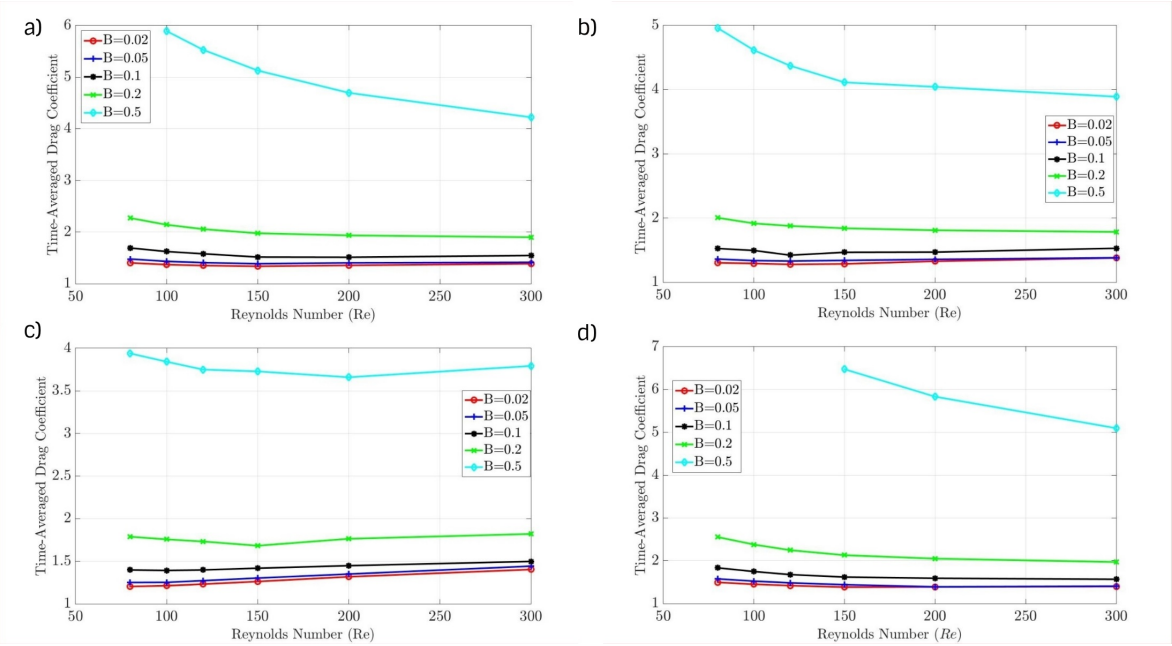

Figure 3.22. Blockage effect on time averaged drag coefficient (C_D) for a) $n = 1$ b) $n = 0.8$ c) $n = 0.6$ d) $n = 1.2$

There are quite few experimental and numerical studies about wall effects on drag reduction and wake formation in the literature for different blockage ratios. Wall effect on drag coefficient is indicated in Figure 3.22 by plotting drag coefficient with respect to Reynolds number for different power-law indices, and it is clearly seen that drag coefficient is enhanced with blockage effect. This outcome is common in many studies in the literature [31, 38, 76].

The role of blockage ratio on the flow of shear-thinning and shear-thickening fluids over a circular cylinder is investigated numerically with the Reynolds number ranging from $Re = 80$ to $Re = 300$. It is found that time-averaged drag coefficient enhances with increasing blockage ratio for both shear-thinning and shear-thickening fluids. Moreover, the trend of vortex shedding frequencies (Strouhal numbers) are parallel to time-averaged drag variations with Reynolds number and blockage ratio. It is also noticed (Figure 3.23) that Strouhal number increases with the increasing blockage ratio which is also observed numerically in other studies [30, 38]. In addition, separation angles are nearly equivalent for each blockage ratios except $B = 0.5$ which

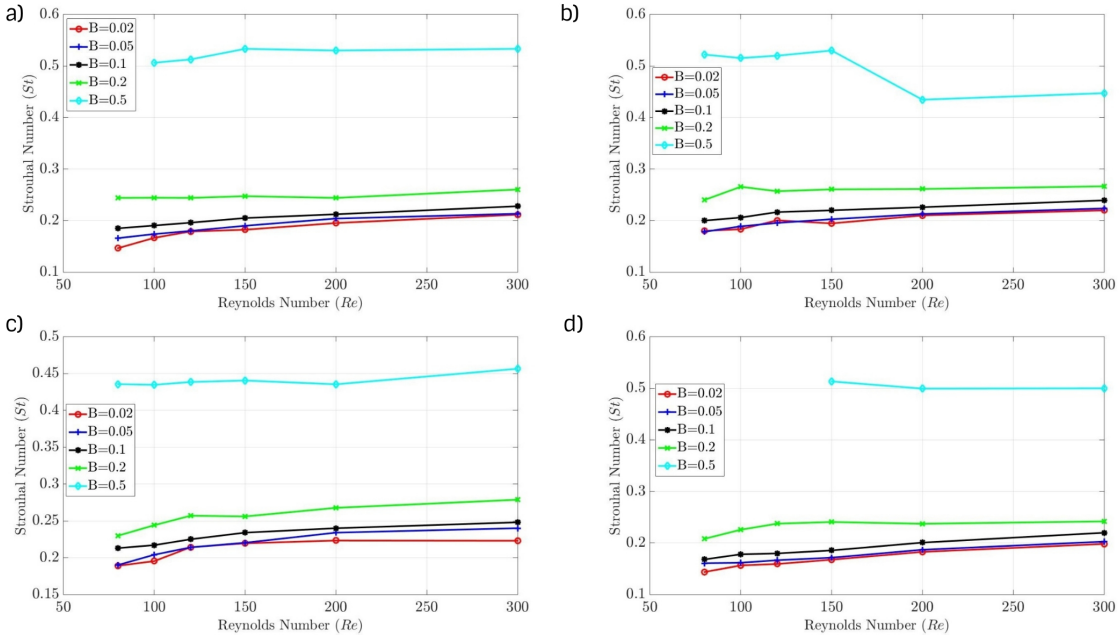

Figure 3.23. Blockage effect on Strouhal Number (St) for a) $n = 1$ b) $n = 0.8$ c) $n = 0.6$ d) $n = 1.2$

has obviously higher values for all Reynolds numbers.

The onset of vortex shedding is also delayed with increasing blockage ratio; besides, shear-thinning effect reduces the critical Reynolds number for the onset of laminar vortex shedding (Re_c) in case of high blockage ratios particularly, while shear-thickening increases the critical Reynolds number as seen in Figure 3.24.

3.2. Non-isothermal Flow Calculations

Although there are some non-isothermal experimental investigations for unconfined non-Newtonian flow past a circular cylinder, existing few numerical studies deal mostly with inelastic fluids, and do not take into account the viscoelastic properties of polymer/surfactant solutions. In this subsection, the unconfined non-isothermal flow past a circular cylinder with both inelastic and viscoelastic non-Newtonian properties is considered in the vortex shedding regime under uniform wall temperature conditions. Instantaneous isotherm profiles, time averaged local Nusselt numbers ($Nu(\theta)$)

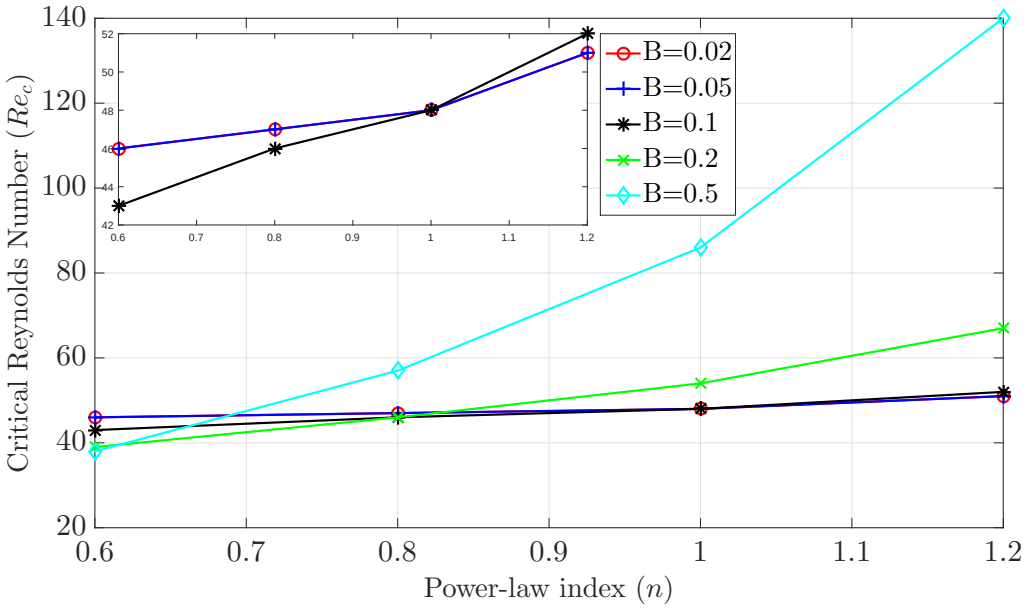

Figure 3.24. Dependence of the critical Reynolds number (Re_c) for the onset of vortex shedding on blockage ratio (B) and power-law index (n).

and surface averaged Nusselt numbers ($\overline{Nu}$) are discussed in detail.

3.2.1. Local Nusselt Number

In Figure 3.25, the local heat transfer rates in terms of the time averaged local Nusselt number values are plotted and compared for the studied fluid models at different Reynolds numbers in the vortex shedding flow regime. For a dilute polymeric solution, the mobility factor and the extensibility parameter are chosen as $\alpha = 0.1$ and $L = 10$ for FENE-P and Giesekus models, respectively. While the maximum local Nusselt number values are located between $\theta = 0$ and $\theta = 50$ degrees, the minimum values are located between $\theta = 110$ and $\theta = 130$ degrees on the cylinder surface.

In general, purely viscoelastic effect (displayed by the Oldroyd-B model) decreases the local values of Nusselt number while inelastic shear thinning behavior (represented by the power-law model) leads to an increase in the local Nusselt numbers compared to Newtonian model. The local Nusselt number values obtained from the Giesekus and

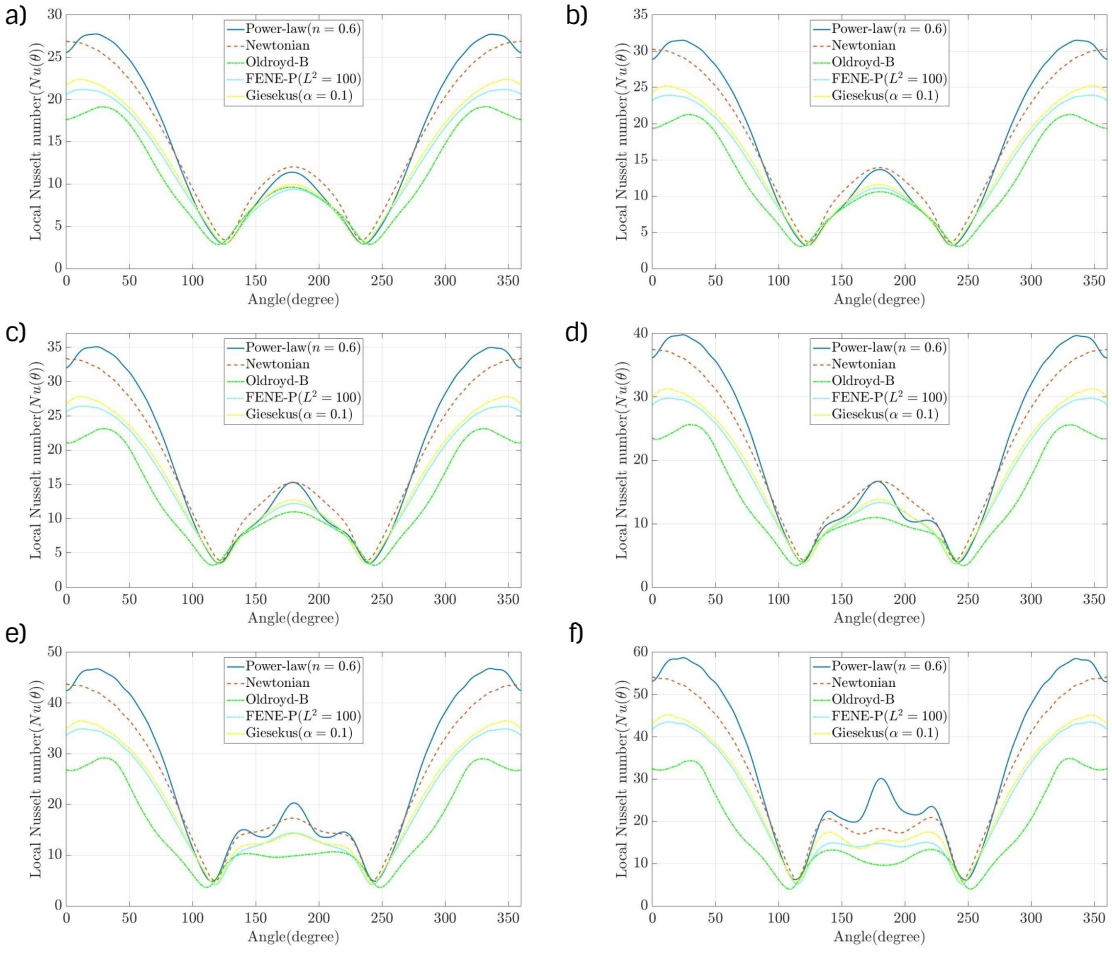

Figure 3.25. Local Nusselt number variation for different models at $Pr = 10$, and $Wi = 1$ (for viscoelastic models) a) $Re = 80$ b) $Re = 100$ c) $Re = 120$ d) $Re = 150$ e) $Re = 200$ f) $Re = 300$

FENE-P models which exhibit combined elastic and shear thinning effects are situated between these purely inelastic and viscoelastic results.

These results may be attributed to the increase in the heat transfer coefficient due to the decrease in apparent viscosity for shear thinning fluids in the boundary layer next to the cylinder surface, where large velocity gradients are observed. It can also be deduced from Figure 3.25 that the heat transfer enhancement for shear thinning power-law fluids or the heat transfer deterioration for viscoelastic Oldroyd-B fluid increase with Reynolds number from laminar to transitional vortex shedding. It can be argued that elasticity plays a role in the stabilization of the flow in vortex shedding through

Table 3.3. Values and locations of the maximum local Nusselt numbers on the cylinder surface for different models ($Wi = 1$ for viscoelastic cases).

	$Re = 80$		$Re = 100$		$Re = 120$		$Re = 150$		$Re = 200$		$Re = 300$	
Models	θ	$Nu(\theta)$	θ	$Nu(\theta)$	θ	$Nu(\theta)$	θ	$Nu(\theta)$	θ	$Nu(\theta)$	θ	$Nu(\theta)$
Giesekus												
$\alpha = 0.1$	11.2	22.40	11.4	25.24	11.5	27.82	11.7	31.31	11.9	36.49	12.1	45.24
$\alpha = 0.01$	12.2	21.96	12.5	24.75	12.7	27.30	12.8	30.76	12.9	35.89	13.2	44.52
$\alpha = 0.001$	24.8	20.61	25.1	23.20	25.3	25.60	25.5	28.84	25.5	33.70	25.6	41.86
FENE-P												
$L^2 = 100$	13.1	21.20	13.2	23.93	13.3	26.42	13.4	29.82	13.4	34.91	13.5	43.52
$L^2 = 400$	24.8	20.19	25.1	22.72	25.2	25.03	25.3	28.18	25.4	32.92	25.4	41.04
$L^2 = 1000$	26.4	19.73	26.8	22.08	26.9	24.28	27.5	27.19	27.3	31.54	27	38.81
Oldroyd-B	28.2	19.13	28.7	21.25	29.2	23.14	30.3	25.65	29.7	29.17	30.1	34.34
Power-law												
$n = 0.6$	23.5	27.75	23.7	31.52	24.0	35.09	24.2	39.82	24.3	46.76	24.5	58.73
$n = 0.8$	14.0	24.4	14.2	27.64	14.3	30.56	14.4	34.57	14.6	40.48	14.6	50.57
Newtonian	0	26.89	0	30.28	0	33.36	0	37.54	0	43.77	0	54.20

a decrease in vortex shedding frequency [18] and an increase in the vortex formation length which in turn leads to a decrease in heat transfer rate near the cylinder surface.

Table 3.3, where values and locations of the maximum local Nusselt numbers on the cylinder surface are shown for different models, indicates that increasing the Reynolds number (Re) leads to an increase in the local heat transfer rate, as also known from the literature [46]. It can be observed from Table 3.2 that the location of the maximum local Nusselt number moves upstream and its value increases with the mobility factor (α) under increased shear thinning. The opposite effect is observed with the increase in the extensibility parameter (L) of FENE-P model (decrease in shear thinning), i.e. the maximum Nusselt number location moves downstream and its value decreases. The lowest values and the closest locations to the rear stagnation point for the maximum local Nusselt number are obtained for purely viscoelastic Oldroyd-B solutions, while inelastic shear thinning power-law solutions display higher maximum local Nusselt number values than purely viscous Newtonian and viscoelastic solutions.

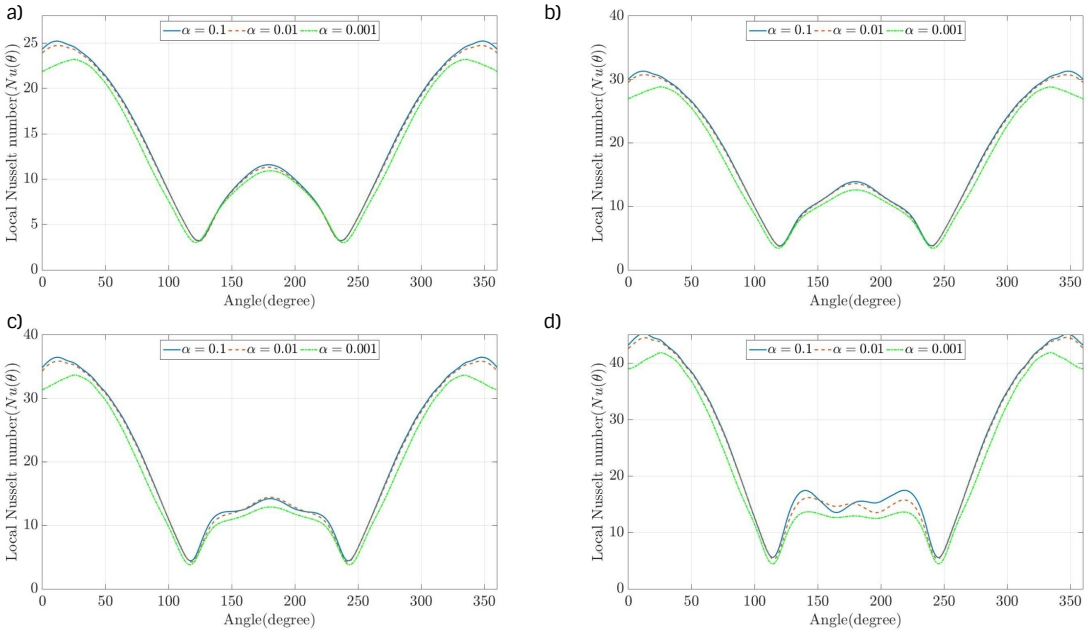

Figure 3.26. The local Nusselt number variation of Giesekus model with $Pr = 10$, $Wi = 1$, a) $Re = 100$ b) $Re = 150$ c) $Re = 200$ d) $Re = 300$

Therefore, decreasing the power-law index (n) increases the maximum local Nusselt number at a fixed Reynolds number. Moreover, the maximum local Nusselt number location is at the front stagnation point for Newtonian fluids.

Time averaged local Nusselt number variations over a surface of the circular cylinder are plotted with the angle in a counterclockwise direction from the front stagnation point (0 or 360 degree) for several mobility factors and extensibility parameters in Figure 3.26 and Figure 3.27. It is shown that increasing mobility factor (α) leads to an increase in the local Nusselt number ($Nu(\theta)$) over the surface of the cylinder as seen in Figure 3.26. Accordingly, Figure 3.27 indicates decreasing extensibility parameter (L) causes to an increase in the local Nusselt number.

3.2.2. Average Nusselt Number

In Figure 3.28, a comparison of the studied models reveal that shear thinning fluids ($n = 0.6$) have highest average Nusselt number ($\overline{Nu}$) values while Oldroyd-B

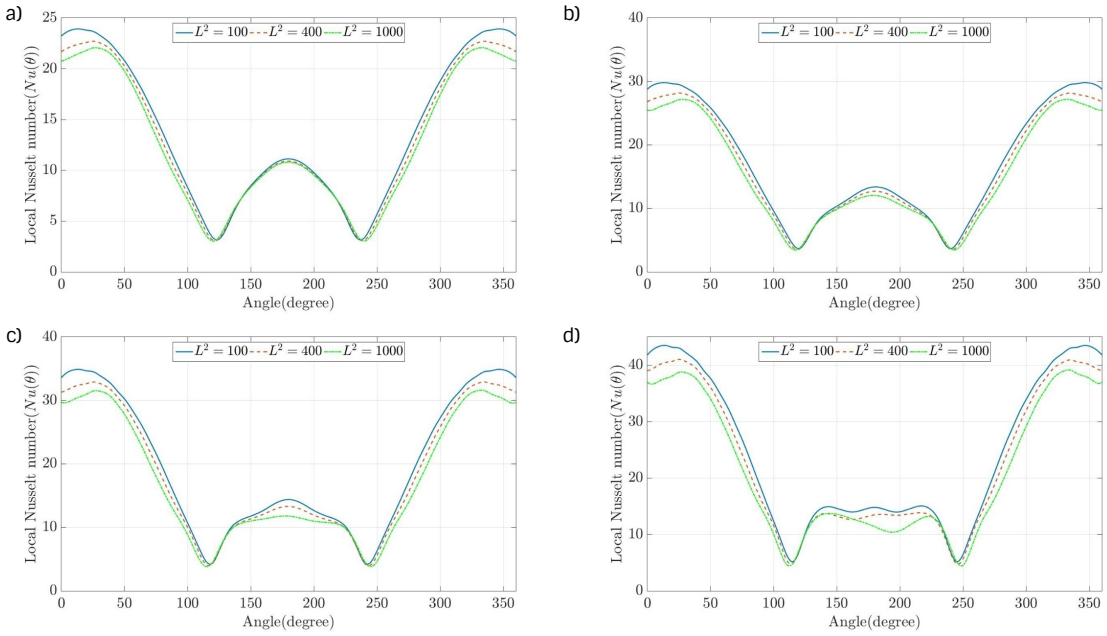

Figure 3.27. The local Nusselt number variation of FENE-P model with $Pr = 10$, $Wi = 1$, a) $Re = 100$ b) $Re = 150$ c) $Re = 200$ d) $Re = 300$

fluids ($Wi = 1$) have lowest values for Reynolds numbers in the range of $80 \leq Re \leq 300$. As suggested in the numerical study of Patnana *et al.* [54], shear thinning behaviour promotes the convective heat transfer, and decreasing power-law index leads to increase in the heat transfer rate. Moreover, Giesekus fluid ($\alpha = 0.1, Wi = 1$) has slightly higher average Nusselt number values whereas FENE-P fluid ($L^2 = 100, Wi = 1$) has lower average Nusselt number values compared to Newtonian case.

In parallel with the local Nusselt numbers, Figure 3.29a demonstrates that average Nusselt number values increase with increasing mobility factor (α) of Giesekus model for all range of Reynolds numbers. Similarly, increasing the extensibility parameter (L) of FENE-P model decreases the average Nusselt number for a fixed value of the Reynolds number as seen in Figure 3.29b.

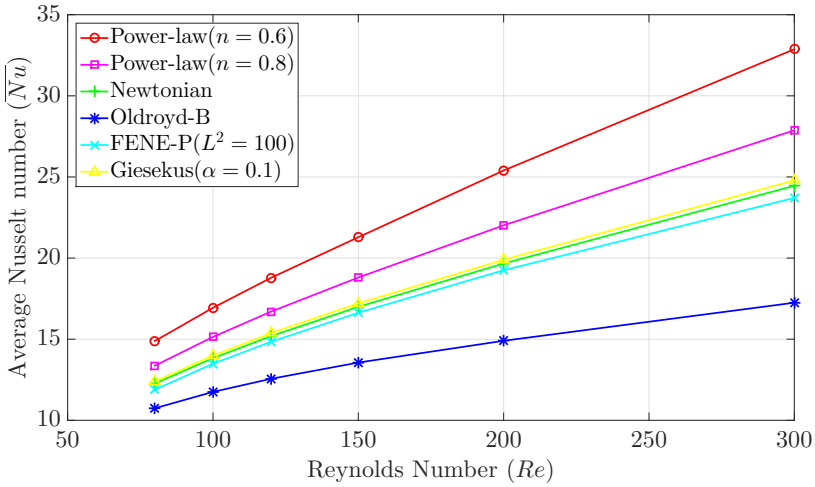

Figure 3.28. Average Nusselt number ($\overline{Nu}$) variation with Reynolds number (Re) for different models ($Wi = 1$ for Oldroyd-B, FENE-P and Giesekus fluids).

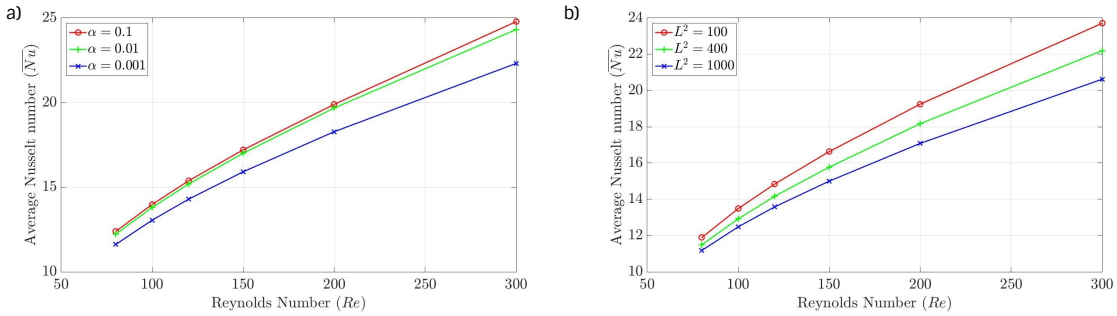

Figure 3.29. a) The effect of the mobility factor (α) on the average Nusselt number ($\overline{Nu}$) variation with Reynolds number (Re) for Giesekus model. b) The effect of the extensibility parameter (L) on the average Nusselt number ($\overline{Nu}$) variation with Reynolds number (Re) for FENE-P model.

3.2.3. Isotherm Contours

Isotherm contours in the wake region of the cylinder are displayed for the studied fluid models at different Reynolds numbers to reveal the variations in the temperature field structure and its effects on convective heat transfer properties. Since the flow is oscillating in time, all isotherms are captured at the instant when the lift coefficient reaches the peak value in steady periodic oscillation for each case. In Figure 3.30,

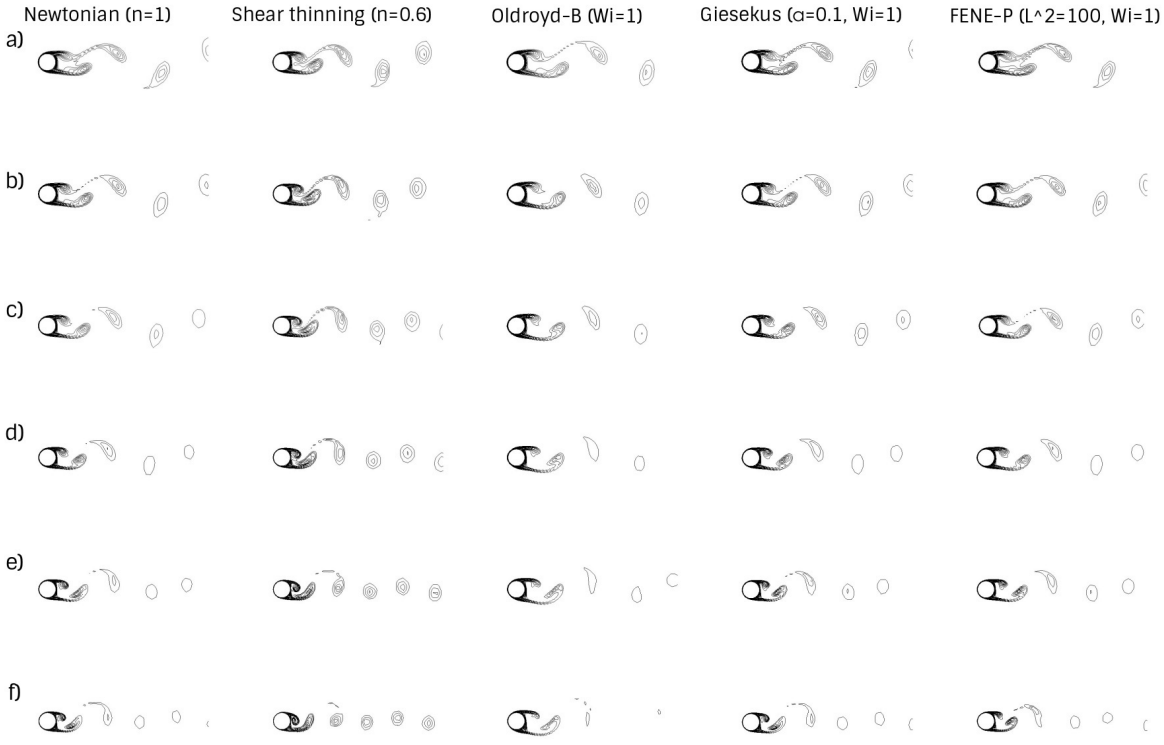

Figure 3.30. Isotherm patterns for different models and Reynolds numbers at $Pr = 10$ a) $Re = 80$ b) $Re = 100$ c) $Re = 120$ d) $Re = 150$ e) $Re = 200$ f) $Re = 300$

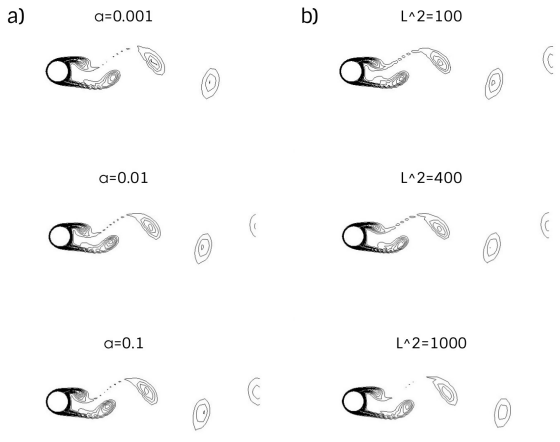

Figure 3.31. Isotherm patterns for Giesekus model with different mobility factors. b) Isotherm patterns for FENE-P model with different finite extensibility parameters $(Re = 100, Wi = 1, Pr = 10)$.

the constant temperature lines for different models are presented for the Reynolds number range of $80 \leq Re \leq 300$. It is shown that the size of the thermal wake (both in length and width) decreases with increasing Reynolds number, from $Re = 80$ to $Re = 300$. More formed isotherm patterns appear under shear thinning in comparison with Newtonian case, whereas clustered pairs are relatively attenuated at high Reynolds numbers under purely elastic effects. The FENE-P and Giesekus isotherms are quite similar to the wake pattern of the Newtonian case, for the chosen values of model parameters.

The temperature gradients in the boundary layer near the cylinder surface are observed to increase under shear thinning and decrease under elasticity, with respect to Newtonian case. This trend is in parallel with the heat transfer enhancement for shear thinning fluids and heat transfer deterioration for elastic fluids, respectively, reflected in the local and average values of the Nusselt number presented in the previous subsections 3.2.1 and 3.2.2.

The effects of the mobility factor (α) and the finite extensibility parameter (L) on the isotherm patterns are illustrated in Figure 3.31a and in Figure 3.31b. It is revealed that decreasing the mobility factor or increasing the extensibility parameter lead to a slight decrease in the temperature gradients and to the attenuation of the thermal wake behind the cylinder due to decreasing shear thinning behavior.

4. CONCLUSION

In this study, a detailed investigation of non-Newtonian effects on two-dimensional unbounded flow around a circular cylinder has been carried out for the vortex shedding and transition regimes, using finite element based numerical simulations. Inelastic and weakly elastic non-Newtonian effects on the flow structure have been revealed in terms of several flow parameters such as drag and lift coefficients, the vortex shedding frequency, the vortex formation length, the separation angle and the critical Reynolds number for the onset of vortex shedding. Purely inelastic shear thinning and purely elastic effects are monitored by the power-law and Oldroyd-B model simulations. Effects of combined shear thinning and elasticity are shown based on Giesekus and FENE-P models which exhibit shear thinning and bounded elongational viscosity through mobility and finite extensibility parameters, respectively.

Drag reduction together with a decrease in the vortex formation length and an increase in shedding frequency is observed under shear thinning, whereas weakly elastic effects lead to increase in drag together with an increase in the formation length and a decrease in vortex shedding frequency. Although shear thinning reduces the separation angle leading to an increase in the pressure (form) drag component, the total drag is reduced due to decrease in the friction (viscous) drag component. For purely elastic case, the separation angle decreases and both the pressure and friction drag components increase. The critical Reynolds number for the onset of periodic flow decreases with shear-thinning, on the contrary it is delayed under shear-thickening, and it is observed that weak elasticity has almost no effect on this onset. Nonetheless, blockage effect increases the drag coefficient and Strouhal number and it delays the onset of laminar vortex shedding for all cases.

Inelastic and weakly elastic effects of dilute polymer/surfactant solutions on the temperature field and convective heat transfer properties are revealed. Both local and average Nusselt number values show that increasing shear thinning effect leads to an enhancement in the rate of convective heat transfer, however significant decrease

in the heat transfer rate is observed under pure elasticity. Increasing the mobility factor of the Giesekus or decreasing the extensibility parameter of the FENE-P models, corresponding also to an increase in shear thinning behavior, leads to an increase in the local Nusselt number on the cylinder surface, and to the shift of the location of the maximum local Nusselt number towards the front stagnation point. Isotherm patterns show that the thermal wake is more pronounced under shear thinning while it is attenuated under elastic effects. The temperature gradients in the boundary layer next to the surface are much higher for shear thinning compared to Newtonian case, whereas they decrease under elasticity.

Even though numerous works have been carried out related to drag reduction by polymer/surfactant additives, mechanism of the drag reduction is still not clear. More extensive experimental and theoretical research are needed for both internal and external flow applications in laminar, transitional and turbulent flow regimes. The effects of these additives on heat transfer properties in non-isothermal flows need to be investigated in more detail as well. It would also be interesting to identify new drag reducers such as polymer added nanofluids (POLY-nanofluid [1]) to improve the drag reduction and heat transfer enhancement. Also, the development of software and computer systems may enable the realistic 3D flow simulations using macro,micro or molecular and atomistic scale modeling.

REFERENCES

1. Tiong, A. N. T., P. Kumar and A. Saptoro, "Reviews on drag reducing polymers", *Korean Journal of Chemical Engineering*, Vol. 32, No. 8, pp. 1455–1476, 2015.

2. Toms, B. A., "Some observations on the flow of linear polymer solutions through straight tubes at large Reynolds numbers", *Proceedings of the 1st International Congress on Rheology*, Vol. 2, pp. 135–141, North-Holland Amsterdam, 1948.

3. Burger, E. D., W. R. Munk, H. A. Wahl *et al.*, "Flow increase in the Trans Alaska Pipeline through use of a polymeric drag-reducing additive", *Journal of Petroleum Technology*, Vol. 34, No. 02, pp. 377–386, 1982.

4. Gadd, G., "Effects of long-chain molecule additives in water on vortex streets", *Nature*, Vol. 211, No. 5045, pp. 169–170, 1966.

5. Fabula, A. G., J. H. Green and W. F. Madison, "Torpedo drag reduction employing polymer ejection", United States Patent, Feb. 5 1980, 4186679.

6. Irgens, F., *Rheology and non-Newtonian fluids*, Springer, 2014.

7. Chhabra, R. P. and J. F. Richardson, *Non-Newtonian flow and applied rheology: engineering applications*, Butterworth-Heinemann, 2011.

8. Chhabra, R. P., "Non-Newtonian fluids: an introduction", *Rheology of complex fluids*, pp. 3–34, Springer, 2010.

9. Bird, R. B., R. C. Armstrong, O. Hassager and C. F. Curtiss, *Dynamics of polymeric liquids*, Vol. 1, Wiley New York, 1977.

10. Kalashnikov, V. and A. Kudin, "Kármán vortices in the flow of drag-reducing polymer solutions", *Nature*, Vol. 225, No. 5231, pp. 445–446, 1970.

11. Usui, H., T. Shibata and Y. Sano, "Kármán vortex behind a circular cylinder in dilute polymer solutions", *Journal of Chemical Engineering of Japan*, Vol. 13, No. 1, pp. 77–79, 1980.

12. Bergins, C., M. Nowak and M. Urban, "The flow of a dilute cationic surfactant solution past a circular cylinder", *Experiments in fluids*, Vol. 30, No. 4, pp. 410–417, 2001.

13. Ozgoren, M., "Flow structure in the downstream of square and circular cylinders", *Flow Measurement and Instrumentation*, Vol. 17, No. 4, pp. 225–235, 2006.

14. Rehimi, F., F. Aloui, S. B. Nasrallah, L. Doubliez and J. Legrand, "Experimental investigation of a confined flow downstream of a circular cylinder centred between two parallel walls", *Journal of Fluids and structures*, Vol. 24, No. 6, pp. 855–882, 2008.

15. Williamson, C. H., "Vortex dynamics in the cylinder wake", *Annual review of fluid mechanics*, Vol. 28, No. 1, pp. 477–539, 1996.

16. He, G. S., N. Li and J. J. Wang, "Drag reduction of square cylinders with cut-corners at the front edges", *Experiments in fluids*, Vol. 55, No. 6, p. 1745, 2014.

17. Coelho, P. and F. Pinho, "Vortex shedding in cylinder flow of shear-thinning fluids: I. Identification and demarcation of flow regimes", *Journal of Non-Newtonian Fluid Mechanics*, Vol. 110, No. 2, pp. 143 – 176, 2003.

18. Coelho, P. and F. Pinho, "Vortex shedding in cylinder flow of shear-thinning fluids: II. Flow characteristics", *Journal of Non-Newtonian Fluid Mechanics*, Vol. 110, No. 2, pp. 177 – 193, 2003.

19. Coelho, P. and F. Pinho, "Vortex shedding in cylinder flow of shear-thinning fluids. III: Pressure measurements", *Journal of Non-Newtonian Fluid Mechanics*, Vol. 121, No. 1, pp. 55 – 68, 2004.

20. Ogata, S., Y. Osano and K. Watanabe, "Effect of surfactant solutions on the drag and the flow pattern of a circular cylinder", *AIChE journal*, Vol. 52, No. 1, pp. 49–57, 2006.

21. Pipe, C. and P. Monkewtiz, "Vortex shedding in flows of dilute polymer solutions", *Journal of non-newtonian fluid mechanics*, Vol. 139, No. 1, pp. 54–67, 2006.

22. Kim, J. T., C. Am Kim, K. Zhang, C. H. Jang and H. J. Choi, "Effect of polymer–surfactant interaction on its turbulent drag reduction", *Colloids and Surfaces A: Physicochemical and Engineering Aspects*, Vol. 391, No. 1, pp. 125–129, 2011.

23. Matras, Z., T. Malcher and B. Gzyl-Malcher, "The influence of polymer–surfactant aggregates on drag reduction", *Thin Solid Films*, Vol. 516, No. 24, pp. 8848–8851, 2008.

24. Patnana, V. K., R. P. Bharti and R. P. Chhabra, "Two-dimensional unsteady flow of power-law fluids over a cylinder", *Chemical Engineering Science*, Vol. 64, No. 12, pp. 2978–2999, 2009.

25. Soares, A., J. Ferreira and R. Chhabra, "Flow and forced convection heat transfer in crossflow of non-Newtonian fluids over a circular cylinder", *Industrial & Engineering Chemistry Research*, Vol. 44, No. 15, pp. 5815–5827, 2005.

26. Sivakumar, P., R. P. Bharti and R. Chhabra, "Effect of power-law index on critical parameters for power-law flow across an unconfined circular cylinder", *Chemical Engineering Science*, Vol. 61, No. 18, pp. 6035–6046, 2006.

27. Chhabra, R., A. Soares and J. Ferreira, "Steady non–Newtonian flow past a circular cylinder: a numerical study", *Acta Mechanica*, Vol. 172, No. 1, pp. 1–16, 2004.

28. Rao, P. K., A. K. Sahu and R. Chhabra, "Flow of Newtonian and power-law fluids past an elliptical cylinder: a numerical study", *Industrial & Engineering Chemistry Research*, Vol. 49, No. 14, pp. 6649–6661, 2010.

29. Sahu, A. K., R. Chhabra and V. Eswaran, "Two-dimensional unsteady laminar flow of a power law fluid across a square cylinder", *Journal of Non-Newtonian Fluid Mechanics*, Vol. 160, No. 2, pp. 157–167, 2009.

30. Anagnostopoulos, P., G. Iliadis and S. Richardson, "Numerical study of the blockage effects on viscous flow past a circular cylinder", *International Journal for Numerical Methods in Fluids*, Vol. 22, No. 11, pp. 1061–1074, 1996.

31. Sahin, M. and R. G. Owens, "A numerical investigation of wall effects up to high blockage ratios on two-dimensional flow past a confined circular cylinder", *Physics of Fluids (1994-present)*, Vol. 16, No. 5, pp. 1305–1320, 2004.

32. Kumar, B. and S. Mittal, "Effect of blockage on critical parameters for flow past a circular cylinder", *International journal for numerical methods in fluids*, Vol. 50, No. 8, pp. 987–1001, 2006.

33. Griffith, M. D., J. Leontini, M. C. Thompson and K. Hourigan, "Vortex shedding and three-dimensional behaviour of flow past a cylinder confined in a channel", *Journal of Fluids and Structures*, Vol. 27, No. 5, pp. 855 – 860, 2011, iUTAM Symposium on Bluff Body Wakes and Vortex-Induced Vibrations (BBVIV-6).

34. Huang, P. and J. Feng, "Wall effects on the flow of viscoelastic fluids around a circular cylinder", *Journal of non-newtonian fluid mechanics*, Vol. 60, No. 2, pp. 179–198, 1995.

35. Oliveira, P. J., "Method for time-dependent simulations of viscoelastic flows: vortex shedding behind cylinder", *Journal of Non-Newtonian Fluid Mechanics*, Vol. 101, No. 1, pp. 113 – 137, 2001.

36. Xiong, Y. L., C.-H. Bruneau and H. Kellay, "A numerical study of two dimensional flows past a bluff body for dilute polymer solutions", *Journal of Non-Newtonian Fluid Mechanics*, Vol. 196, pp. 8–26, 2013.

37. Norouzi, M., S. Varedi, M. Maghrebi and M. Shahmardan, "Numerical investigation of viscoelastic shedding flow behind a circular cylinder", *Journal of Non-Newtonian Fluid Mechanics*, Vol. 197, No. Supplement C, pp. 31 – 40, 2013.

38. Rao, M., A. K. Sahu and R. Chhabra, "Effect of confinement on power-law fluid flow past a circular cylinder", *Polymer Engineering & Science*, Vol. 51, No. 10, pp. 2044–2065, 2011.

39. Kim, N.-J., S. Kim, S. H. Lim, K. Chen and W. Chun, "Measurement of drag reduction in polymer added turbulent flow", *International Communications in Heat and Mass Transfer*, Vol. 36, No. 10, pp. 1014–1019, 2009.

40. McComb, W. and L. Rabie, "Local drag reduction due to injection of polymer solutions into turbulent flow in a pipe. Part I: Dependence on local polymer concentration", *AIChE Journal*, Vol. 28, No. 4, pp. 547–557, 1982.

41. Toh, K. H. and A. J. Ghajar, "Heat transfer in the thermal entrance region for viscoelastic fluids in turbulent pipe flows", *International journal of heat and mass transfer*, Vol. 31, No. 6, pp. 1261–1267, 1988.

42. Hartnett, J. P., "1990 Max Jakob Memorial Award Lecture: Viscoelastic Fluids: A New Challenge in Heat Transfer", *Journal of Heat Transfer*, Vol. 114, No. 2, pp. 296–303, 1992.

43. Gao, S. and J. Hartnett, "Heat transfer behavior of Reiner-Rivlin fluids in rectangular ducts", *International journal of heat and mass transfer*, Vol. 39, No. 6, pp. 1317–1324, 1996.

44. Rao, B., "Laminar mixed convection heat transfer to viscoelastic fluids in a 5: 1 rectangular channel", *International Journal of Heat and Fluid Flow*, Vol. 10, No. 4, pp. 334–338, 1989.

45. Xie, C. and J. P. Hartnett, "Influence of rheology on laminar heat transfer to

viscoelastic fluids in a rectangular channel", *Industrial & engineering chemistry research*, Vol. 31, No. 3, pp. 727–732, 1992.

46. Chhabra, R., "Fluid flow and heat transfer from circular and noncircular cylinders submerged in non-Newtonian liquids", *Advances in Heat Transfer*, Vol. 43, pp. 289–417, Elsevier, 2011.

47. Shah, M., E. Petersen and A. Acrivos, "Heat transfer from a Cylinder to a Power-law Non-Newtonian Fluid", *AIChE Journal*, Vol. 8, No. 4, pp. 542–549, 1962.

48. James, D. F. and A. J. Acosta, "The laminar flow of dilute polymer solutions around circular cylinders", *Journal of Fluid Mechanics*, Vol. 42, No. 2, pp. 269–288, 1970.

49. Ghosh, U., S. Gupta, S. Kumar and S. Upadhyay, "Mass transfer in cross flow of non-Newtonian fluid around a circular cylinder", *International journal of heat and mass transfer*, Vol. 29, No. 6, pp. 955–960, 1986.

50. Ghosh, U., S. Upadhyay and R. Chhabra, "Heat and mass transfer from immersed bodies to non-Newtonian fluids", *Advances in Heat Transfer*, Vol. 25, pp. 252–321, 1994.

51. Hoyt, J. and R. Sellin, "Cylinder cross-flow heat transfer in drag-reducing fluid", *Experimental Heat Transfer*, Vol. 2, No. 2, pp. 113–127, 1989.

52. Rao, B., "Heat transfer to non-Newtonian flows over a cylinder in cross flow", *International journal of heat and fluid flow*, Vol. 21, No. 6, pp. 693–700, 2000.

53. Bharti, R. P., R. Chhabra and V. Eswaran, "Steady forced convection heat transfer from a heated circular cylinder to power-law fluids", *International Journal of Heat and Mass Transfer*, Vol. 50, No. 5-6, pp. 977–990, 2007.

54. Patnana, V. K., R. P. Bharti and R. P. Chhabra, "Two-dimensional unsteady

forced convection heat transfer in power-law fluids from a cylinder", *International Journal of Heat and Mass Transfer*, Vol. 53, No. 19-20, pp. 4152–4167, 2010.

55. Lumley, J. L., "Drag reduction by additives", *Annual review of fluid mechanics*, Vol. 1, No. 1, pp. 367–384, 1969.

56. Landahl, M. T., "Drag reduction by polymer addition", *Theoretical and Applied Mechanics*, pp. 177–199, Springer, 1973.

57. De Gennes, P.-G., *Introduction to polymer dynamics*, CUP Archive, 1990.

58. Joseph, D. D., A. Narain and O. Riccius, "Shear-wave speeds and elastic moduli for different liquids. Part 1. Theory", *Journal of Fluid Mechanics*, Vol. 171, p. 289–308, 1986.

59. Joseph, D. D., *Fluid dynamics of viscoelastic liquids*, Vol. 84, Springer-Verlag New York, 1990.

60. Bonn, D., Y. Amarouchene, C. Wagner, S. Douady and O. Cadot, "Turbulent drag reduction by polymers", *Journal of Physics: Condensed Matter*, Vol. 17, No. 14, p. S1195, 2005.

61. Dimitropoulos, C. D., R. Sureshkumar and A. N. Beris, "Direct numerical simulation of viscoelastic turbulent channel flow exhibiting drag reduction: effect of the variation of rheological parameters1", *Journal of Non-Newtonian Fluid Mechanics*, Vol. 79, No. 2-3, pp. 433–468, 1998.

62. Den Toonder, J., M. Hulsen, G. Kuiken and F. Nieuwstadt, "Drag reduction by polymer additives in a turbulent pipe flow: numerical and laboratory experiments", *Journal of Fluid Mechanics*, Vol. 337, pp. 193–231, 1997.

63. Gillissen, J., "Polymer flexibility and turbulent drag reduction", *Physical Review E*, Vol. 78, No. 4, p. 046311, 2008.

64. Kwack, E. and J. Hartnett, "New method to determine characteristic time of viscoelastic fluids", *International Communications in Heat and Mass Transfer*, Vol. 10, No. 1, pp. 77–82, 1983.

65. Kwack, E. Y., J. P. Hartnett and Y. I. Cho, "Turbulent heat transfer in circular tube flows of viscoelastic fluids", *Wärme - und Stoffübertragung*, Vol. 16, No. 1, pp. 35–44, March 1982.

66. Min, T., J. Y. Yoo, H. Choi and D. D. Joseph, "Drag reduction by polymer additives in a turbulent channel flow", *Journal of Fluid Mechanics*, Vol. 486, pp. 213–238, 2003.

67. Kostic, M., "On turbulent drag and heat transfer reduction phenomena and laminar heat transfer enhancement in non-circular duct flow of certain non-Newtonian fluids", *International journal of heat and mass transfer*, Vol. 37, pp. 133–147, 1994.

68. Zdravkovich, M., *Flow around Circular Cylinders: Volume 2: Applications*, Vol. 2, Oxford University Press, 2003.

69. Phan-Thien, N. and N. Mai-Duy, *Understanding viscoelasticity: an introduction to rheology*, Springer, 2017.

70. Purnode, B. and M. Crochet, "Polymer solution characterization with the FENE-P model", *Journal of non-newtonian fluid mechanics*, Vol. 77, No. 1-2, pp. 1–20, 1998.

71. Bhatara, G., E. S. Shaqfeh and B. Khomami, "The influence of polymer concentration and chain architecture on free surface displacement flows of polymeric fluids", *Journal of Rheology*, Vol. 49, No. 5, pp. 929–962, 2005.

72. Rocha, G. N., R. J. Poole, M. A. Alves and P. J. Oliveira, "On extensibility effects in the cross-slot flow bifurcation", *Journal of Non-Newtonian Fluid Mechanics*, Vol. 156, No. 1-2, pp. 58–69, 2009.

73. Peters, G. W. and F. P. Baaijens, "Modelling of non-isothermal viscoelastic flows", *Journal of Non-Newtonian Fluid Mechanics*, Vol. 68, No. 2-3, pp. 205–224, 1997.

74. Polyflow, A., *12.1 user's guide*, Ansys, Inc., 2009.

75. Wieselsberger, C., "New Data on the Laws of Fluid Dynamics", *Physikalische Zeitschrift*, Vol. 22, 1921.

76. Zdravkovich, M., *Flow Around Circular cylinders. A Comprehensive Guide Through Flow Phenomena, Experiments, Applications, Mathematical Models, and Computer Simulations, vol. 1: Fundamentals*, Vol. 1, Oxford University Press, 1997.

77. Perkins, H. C. and G. Leppert, "Forced convection heat transfer from a uniformly heated cylinder", *Journal of Heat Transfer*, Vol. 84, No. 3, pp. 257–261, 1962.

78. Whitaker, S., "Forced convection heat transfer correlations for flow in pipes, past flat plates, single cylinders, single spheres, and for flow in packed beds and tube bundles", *AIChE Journal*, Vol. 18, No. 2, pp. 361–371, 1972.

79. Norberg, C., "Flow around a circular cylinder: aspects of fluctuating lift", *Journal of Fluids and Structures*, Vol. 15, No. 3, pp. 459–469, 2001.

80. Rajani, B., A. Kandasamy and S. Majumdar, "Numerical simulation of laminar flow past a circular cylinder", *Applied Mathematical Modelling*, Vol. 33, No. 3, pp. 1228–1247, 2009.

81. Antonia, R. and S. Rajagopalan, "Determination of drag of a circular cylinder", *AIAA journal*, Vol. 28, No. 10, pp. 1833–1834, 1990.

82. Son, O. and O. Cetiner, "Drag Prediction in the Near Wake of a Circular Cylinder based on DPIV Data.", *Journal of Applied Fluid Mechanics*, Vol. 9, No. 4, pp. 1963–1968, 2016.

83. Gerrard, J., "The wakes of cylindrical bluff bodies at low Reynolds number", *Philosophical Transactions of the Royal Society of London A: Mathematical, Physical and Engineering Sciences*, Vol. 288, No. 1354, pp. 351–382, 1978.

84. Ahlborn, B., M. L. Seto and B. R. Noack, "On drag, Strouhal number and vortex-street structure", *Fluid Dynamics Research*, Vol. 30, No. 6, pp. 379–399, 2002.

85. Norberg, C., "An experimental investigation of the flow around a circular cylinder: influence of aspect ratio", *Journal of Fluid Mechanics*, Vol. 258, pp. 287–316, 1994.

86. Williamson, C., "Oblique and parallel modes of vortex shedding in the wake of a circular cylinder at low Reynolds numbers", *Journal of Fluid Mechanics*, Vol. 206, pp. 579–627, 1989.

87. Lashgari, I., J. O. Pralits, F. Giannetti and L. Brandt, "First instability of the flow of shear-thinning and shear-thickening fluids past a circular cylinder", *Journal of Fluid Mechanics*, Vol. 701, pp. 201–227, 2012.

88. Thoman, D. C. and A. A. Szewczyk, "Time-Dependent Viscous Flow over a Circular Cylinder", *Physics of Fluids (1958-1988)*, Vol. 12, No. 12, pp. II–76, 1969.

89. Wu, M.-H., C.-Y. Wen, R.-H. Yen, M.-C. Weng and A.-B. Wang, "Experimental and numerical study of the separation angle for flow around a circular cylinder at low Reynolds number", *Journal of Fluid Mechanics*, Vol. 515, pp. 233–260, 2004.

90. Gerrard, J., "The mechanics of the formation region of vortices behind bluff bodies", *Journal of Fluid Mechanics*, Vol. 25, No. 02, pp. 401–413, 1966.